Molecular composition and processing of aqueous secondary organic aerosol in clouds at a mountain site in southeastern China

Yali Jin[1,2,3,4], Hao Luo[1,6], Siqi Tang[1], Shuhui Xue[1], Chengyu Nie[1], Xiaocong Peng[7], Yan Zheng[9], Weiqi Xu[8], Guohua Zhang[7], Xiaole Pan[8], Yele Sun[8], Qi Chen[9], Lanzhong Liu[8], and Defeng Zhao[1,3,4,5]

[1]Department of Atmospheric and Oceanic Sciences & Institute of Atmospheric Sciences, Fudan University, Shanghai, 200438, China

[2]Shanghai Frontiers Science Center of Atmosphere-Ocean Interaction, Fudan University, Shanghai, 200438, China

[3]Shanghai Key Laboratory of Ocean-land-atmosphere Boundary Dynamics and Climate Change, Fudan University, Shanghai, 200438, China

[4]National Observations and Research Station for Wetland Ecosystems of the Yangtze Estuary, Fudan University, Shanghai, 200438, China

[5]Institute of Eco-Chongming (IEC), 20 Cuiniao Rd., Chongming, Shanghai, 202162, China

[6]Inner Mongolia Key Laboratory of Pollution Control and Low Carbon Resource Utilization, Inner Mongolia University, Inner Mongolia, 010021, China

[7]State Key Laboratory of Advanced Environmental Technology, Guangzhou Institute of Geochemistry, Chinese Academy of Sciences, Guangzhou, 510640, China

[8]State Key Laboratory of Atmospheric Environment and Extreme Meteorology, Institute of Atmospheric Physics, Chinese Academy of Sciences, Beijing, 100029, China

[9]State Key Laboratory of Regional Environment and Sustainability, College of Environmental Sciences and Engineering, Peking University, Beijing, 100871, China

Corresponding to: Defeng Zhao (dfzhao@fudan.edu.cn)

Abstract. Aqueous secondary organic aerosol (aqSOA) contributes substantially to organic aerosol (OA), affecting air quality, human health, and climate. However, the molecular composition and processing of aqSOA in clouds remain unclear due to limited online field measurements. We measured molecular composition of OA online (time resolution 20 s) and tracked its processing at a mountain site in southeastern China, using an Extractive ElectroSpray Ionization inlet coupled with a Time-of-Flight Mass Spectrometer (EESI-ToF-MS). We identified 2084 molecular formulas and compared OA composition from three sample types: cloud ~~droplets (CD~~droplet residuals (CDR), interstitial aerosol particles (INT), and cloud-free aerosol particles (CF) in representative cloud episodes. CHO class was the dominant constituent, followed by CHON class. In most cloud episodes, the fraction of CHO was lower in ~~CD~~CDR than that in INT and CF, while the fraction of CHON was higher, which may result from the uptake of organonitrates or nitration in cloud water. Compounds in ~~CD~~CDR had more carbon number and higher molecular weight than CF, which is attributed to accretion reactions in cloud water. We identified 39 significantly enriched compounds in ~~CD~~CDR compared with CF, which could be potentially used as aqSOA tracers formed via cloud processing. This study also reveals rapid changes in aqSOA composition, which highlight the necessity for high time resolution measurements to capture the processing of aqSOA in clouds. Overall, this study provides clear information on processing of aqSOA in clouds and highlights the importance of accretion reactions, which have implications on the composition and physicochemical properties of SOA.

1 Introduction

Secondary organic aerosol (SOA) is a major component of organic aerosol (OA) with diverse emission sources, gaseous precursors, and composition, exerting significant impacts on air quality, climate, and human health (Jimenez et al., 2009; Nault et al., 2021). SOA is primarily produced through the oxidation of volatile organic compounds (VOCs), while the atmospheric aging of primary organic aerosol (POA) may also contribute. Numerous previous studies have investigated the formation mechanisms of SOA, with particular emphasis on gas-phase pathways (Odum et al., 1996; Ervens et al., 2011). However, SOA formed solely through gas-phase reactions (gasSOA) cannot fully account for the observed SOA concentrations (de Gouw et al., 2005; Volkamer et al., 2007; Volkamer et al., 2006). In addition to the traditional gas-phase processing, aqueous-phase pathways have been recognized as an important source of SOA (Sehested et al., 1975; Galloway et al., 1976; Graedel and Weschler, 1981; Fu et al., 2008; Tan et al., 2009; Zhang et al., 2010; Ervens et al., 2011; Lamkaddam et al., 2021).

Mounting evidence for aqueous secondary organic aerosol (aqSOA) has been reported in field observations in various atmospheric aqueous systems, i.e., aerosol liquid water (ALW), fog water, and cloud water. For example, several studies on source apportionment in different sites showed that aqSOA formed in ALW is an important contributor to SOA, with its fraction particularly elevated (up to 44 %) under high relative humidity (RH) conditions (Wang et al., 2021; Zhao et al., 2019; Tong et al., 2021; Gilardoni et al., 2016; Duan et al., 2022; Xu et al., 2019; Sun et al., 2016). Relative to ALW, fog water and cloud water are diluted aqueous systems where aqSOA can also be formed (Herckes et al., 2013). For fog water, the ratio of aqSOA to OA during fog-rain days is enhanced compared with non-fog-rain days (Duan et al., 2021). Additionally, OA composition of fog water is more oxidized (Brege et al., 2018), has more N-containing compounds (Mattsson et al., 2025; Sun et al., 2024a; Kim et al., 2019) compared with aerosol particles, and shows signs of oligomerization based on fragments in the mass spectrum (Gilardoni et al., 2016; Mandariya et al., 2019). In contrast to fog, the cloud is more common, ubiquitously presents in the atmosphere, and consists of a large quantity of droplets generated by aerosol activation, providing an aqueous medium for physical processes and chemical reactions (McNeill et al., 2012; McNeill, 2015). Within clouds, aerosol particles may undergo repeated hydration-dehydration cycles, including hygroscopic growth, activation, and subsequent evaporation. Such cloud processing could influence the concentration of OA composition (Wang et al., 2024b; Gao et al., 2023; Liu et al., 2023b), thereby influencing aerosol size distribution, hygroscopicity, volatility, and cloud condensation nuclei (CCN) activity (Jimenez et al., 2009; Sun et al., 2025). Additionally, cloud processing may facilitate the formation of brown carbon, including N-containing heterocyclic compounds, which could affect atmospheric radiative forcing (Liu et al., 2023b).

A number of field campaigns have been conducted to measure the chemical composition of OA in cloud ~~droplets.~~droplet residuals. Several previous field campaigns found that more highly oxygenated OA is present in cloud ~~droplets~~droplet residuals compared to cloud-free aerosol particles using online techniques, Aerosol Mass Spectrometer (AMS) or Aerodyne Aerosol

Chemical Speciation Monitor (ACSM), which provide information on fragment ions of compounds, such as the fraction of m/z 44 (CO_2^+) in the mass spectra (Dadashazar et al., 2022; Lance et al., 2020; Gao et al., 2023). Although these studies provide valuable information on the chemical composition of aqSOA, the use of AMS or ACSM leads to molecular fragmentation and thus cannot provide molecular formulas for the components of aqSOA. As a result, the molecular composition of aqSOA and mechanisms of its formation and transformation remain incompletely understood. This gap hinders the analysis of sources, evolution, health effects, and climate impacts with respect to specific OA compounds.

Molecular formulas of OA in cloud samples can be assigned and classified into several groups, including CHO, CHON, CHOS, and CHONS, with CHO and CHON accounting for the largest fractions (Liu et al., 2023b; Cook et al., 2017; Pailler et al., 2024; Zhao et al., 2013; Bianco et al., 2019; Sun et al., 2021; Gramlich et al., 2023). Oligomers (Cook et al., 2017; Zhao et al., 2013), organosulfates (Sun et al., 2021; Bianco et al., 2019), and N-containing compounds such as nitroaromatics (Sun et al., 2021; Cook et al., 2017; Bianco et al., 2019) have been observed in cloud droplets. Although the molecular composition of OA in cloud droplets has been characterized using offline techniques such as Fourier Transform Ion Cyclotron Resonance Mass Spectrometry (FT-ICR-MS), the formation mechanisms of many compounds in clouds remain uncertain. For example, it is not clear whether the oligomers originate from cloud processing or from aqueous aerosol due to a lack of concomitant aerosol measurements and limited temporal variation analyses (Cook et al., 2017; Zhao et al., 2013). The coarse time resolution of filter-based sampling (several hours to one day), together with limited sample numbers, prevents these studies from resolving cloud-processing reaction processes that occur on minute-to-hour timescales and are subjected to the influence of rapid variability in meteorological conditions within clouds. The chemical characteristics of aqSOA obtained from comparisons between cloud droplets and cloud-free aerosol particles are subject to large uncertainties, because the composition of both cloud droplets and aerosols may change over long-time sampling. Therefore, it is necessary to obtain online molecular information on OA in clouds by comparing OA composition of cloud droplets, interstitial aerosol particles, and cloud-free aerosol particles, to provide new insights into the detailed chemical composition, evolution variation, and the mechanism of cloud processing.

To get a detailed understanding of cloud processing of aqSOA, we measured the real-time molecular composition of aqSOA in clouds using an Extractive ElectroSpray Ionization inlet coupled with a Time-of-Flight Mass Spectrometer (EESI-ToF-MS) in a mountain site in southeastern China. In this study, we identify molecular formulas of OA in cloud processing and compare differences in OA characteristics between cloud ~~droplets (CD~~droplet residuals (CDR), interstitial aerosol particles (INT), and cloud-free aerosol particles (CF). We explore new compounds formed in cloud processing and explain their potential formation mechanisms. We also aim to track the temporal evolution of compounds in aqSOA during cloud processing.

2 Methods

We conducted this field campaign from May 1st to May 29th in 2024 at Shanghuang Eco-Environmental Observatory of Chinese Academy of Sciences at the summit of the Damaojian mountain (119.51° E and 28.58° N, 1128 m above sea level) located in Jinhua city, Zhejiang province, China. The site is a background monitoring station surrounded by coniferous and broad-leaved forests away from megacities, as shown in Fig. 1. In addition to biogenic emissions, this site may be affected by anthropogenic activities originating from the surrounding small counties, as mentioned in Zhang et al. (2024).

Cloud droplets ~~(CD)~~ were collected using a Ground-based Counterflow Virtual Impactor (GCVI, Brechtel Manufacturing Inc., Model 1205). The GCVI collected ~~CD~~cloud droplets with diameters larger than 8.5 μm (Shingler et al., 2012) under conditions of visibility < 3 km, RH > 95 %, and absence of precipitation. After separation from INT (non-activated aerosol in clouds), the ~~CD~~cloud droplets were dried by mild heating (40 °C) within the GCVI (Lin et al., 2017) and further by a Nafion dryer downstream, and ~~the residues of CD~~CDR were subsequently measured. ~~We note that the term "CD" in the Results and Discussion section refers to the residues of cloud droplets.~~ Because the focus is on the relative compositional change of OA in ~~CD~~CDR and CF, the GCVI enhancement factor was not applied. A $PM_{2.5}$ (particulate matter smaller than 2.5 μm) cyclone inlet (URG, USA) was used to collect INT and CF. A switching system alternated between the GCVI and the URG inlet: $PM_{2.5}$ was sampled when GCVI detected no cloud, whereas ~~CD~~CDR sampling was triggered automatically once cloud presence was detected by GCVI. During cloud episodes, the switch was also configured to alternate between ~~CD~~CDR and INT sampling. It should be noted that the terms "cloudy days" and "cloudless days" in this study specifically refer to periods with and without low clouds.

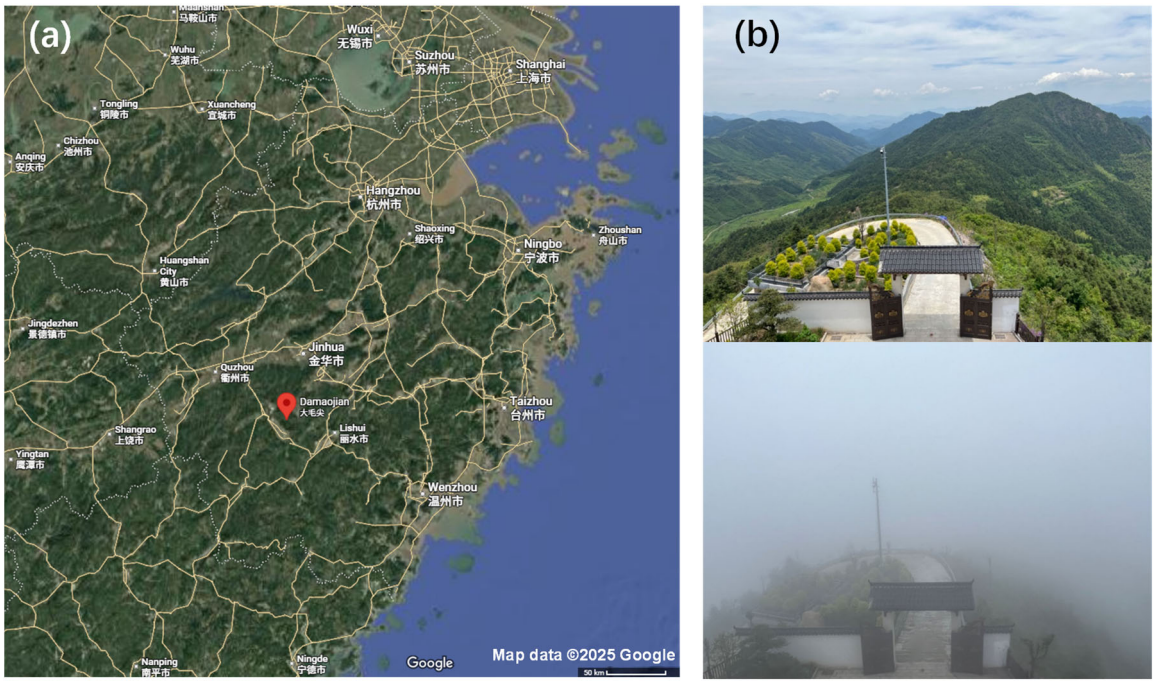

Figure 1. Location of the Shanghuang site. (a) a map (from Google Maps) and (b) two photos of the sampling site, one with cloud and another without cloud.

Measurements of ~~CD~~CDR, INT, and CF were conducted through a manifold positioned downstream of both the GCVI and URG inlets. The concentrations of OA composition were measured online using EESI-ToF-MS (Aerodyne Institute) with a time resolution of 20 s. This mass spectrometer achieves soft ionization while preserving the structure of compounds, measuring molecular formulas with high mass resolution (8000–10000) and low detection limit (Wang et al., 2024a). Detailed information regarding EESI-ToF-MS has been reported previously (Lopez-Hilfiker et al., 2019; Stefenelli et al., 2019; Brown et al., 2021; Kumar et al., 2022; Luo et al., 2024; Xue et al., 2025). Aerosol was sampled after gaseous compounds were removed by entering a charcoal denuder, and subsequently intersected with an electrospray generated from a working solution containing 100 ppm NaI in a 1:1 (v/v) water and acetonitrile mixture, allowing aerosol compounds to be detected as $[M+Na]^+$ in positive ion mode. Background measurements were obtained by switching the inlet to a filter. The durations of sample and background collection can be adjusted to ensure aerosol signal levels return to baseline within the time of background (Qi et al., 2019). In this campaign, the sample and background were set in combinations of 10 min and 5 min typically. The sampling volume of EESI-ToF-MS was 0.9 L m^{-3}. Weekly calibration was performed using levoglucosan, and the sensitivity was assumed identical for all compounds. All organic compound signals are shown as relative intensities normalized to $(NaI)Na^+$ to avoid interference from the ion source fluctuations in EESI-ToF-MS. Mass spectral data were processed using Tofware 3.2.5 in Igor Pro 8. For data screening, the signal-to-background ratio (s/b) was calculated as the median value of (sample signal−background)/background, thereby excluding compounds showing insignificant differences between sample and background. Only compounds with the s/b ratio greater than 0.1 were included (Tong et al., 2021). After this screening, 79, 148, 604, and 126 compounds were retained from cloud episodes one to four, respectively. All results presented in Sect. 3.2 are based on these screened data.

The OA size distribution was characterized using a scanning mobility particle sizer (SMPS, TSI 3936), which, together with an atomizer (TSI, 3076), was used to facilitate EESI-ToF-MS calibration. $PM_{2.5}$ concentration was monitored using a Thermo Scientific instrument (Thermo Scientific. Model 5014i), while CO was measured by a Picarro greenhouse gas analyzer (Picarro Inc., G2401). Meteorological parameters including RH, Temperature (T), wind speed (WS), and wind direction (WD) were monitored by an automatic weather station.

The 72 h backward trajectories of air masses arriving at the Shanghuang site were calculated by the Hybrid Single-Particle Lagrangian Integrated Trajectory (HYSPLIT) model, with Global Data Assimilation System (GDAS) meteorological data at 1°×1° spatial resolution (Stein et al., 2015; Rolph et al., 2017). These trajectories were clustered into several appropriate groups for selected cloud episodes. The clustering was based on the total spatial variance (TSV) method (Song et al., 2023; Roland et al., 2025)~~.~~ in MeteoInfo software (Wang, 2014).

3 Results and discussion

3.1 Characteristics of cloud episodes

During the entire campaign, $PM_{2.5}$ concentration was 13.4±10.8 μg m^{-3} (mean value ± standard deviation), with the highest concentration of 72.2 μg m^{-3} observed on cloudless days, as shown in Fig. 2. The $PM_{2.5}$ concentration is typical in rural areas of China and is substantially lower than that observed in the same season in metropolitan cities such as Beijing (~40 μg m^{-3}) and Shanghai (~30 μg m^{-3}) (Liu et al., 2023a; Yin et al., 2023).

Cloud episodes accounted for 27.1 % of the one-month campaign, with the sample types of ~~CD~~CDR and INT representing 13.1 % and 14.0 %, respectively. Of the 16 recorded cloud episodes, we selected those without precipitation ~~and with adjacent cloud-free periods (<2 h from CD)~~ to avoid the influence of wet deposition and ~~ensure CD/~~with a cloud-free period within <2 h from the cloud episode, and for which CDR, INT~~/~~, and CF ~~sampling coverage~~samples were all available. Six out of 16 episodes meet these criteria, and four cloud episodes (CEs) are further selected. CE1, CE2, CE3, and CE4 differ in $PM_{2.5}$ and CO concentration, meteorological conditions, origin of air mass, and duration time, as shown in Table S1. The duration of each CE ranged from several minutes to three days. Meteorological conditions and origin of air masses are discussed in Text S1, and backward trajectories from HYSPLIT are shown in Fig. S2.

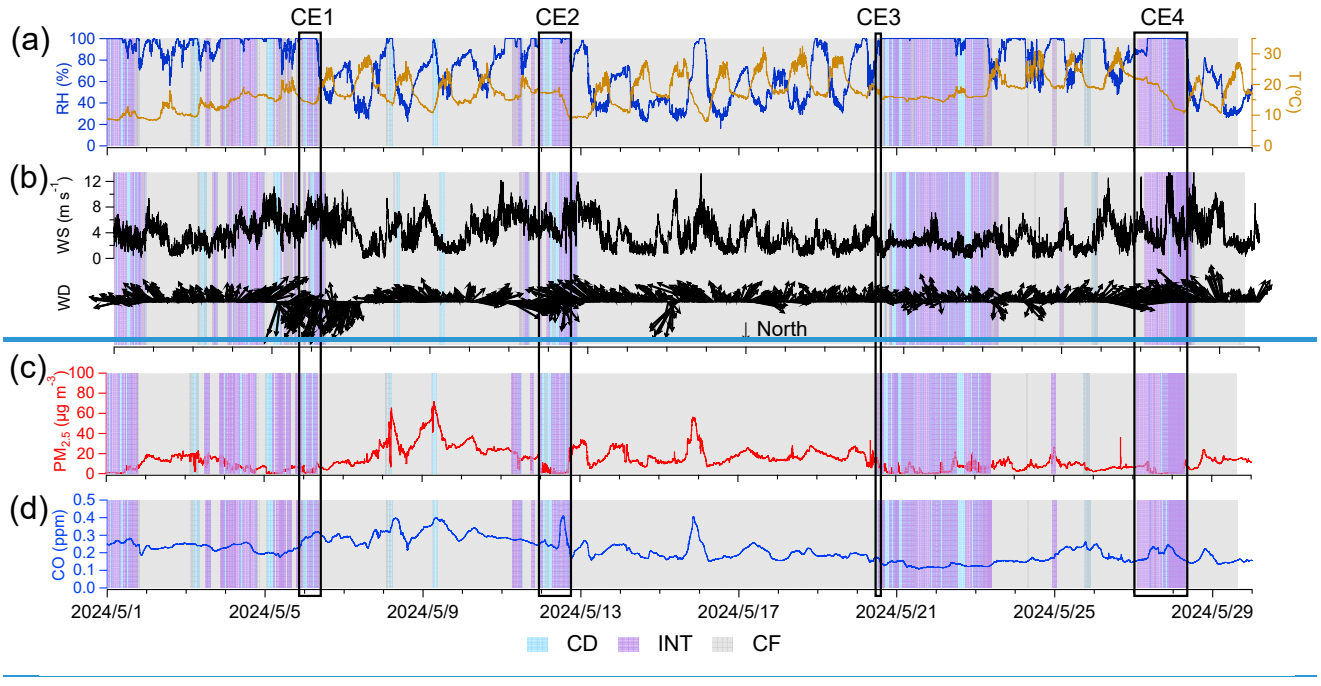

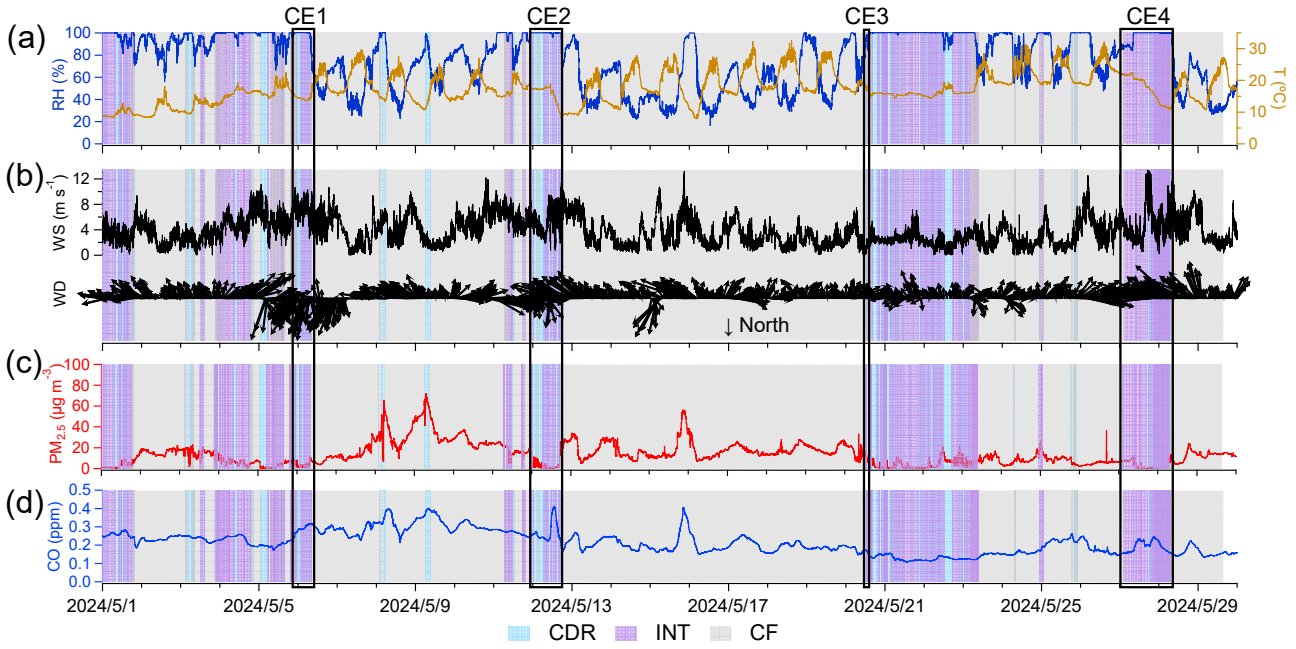

Figure 2. Time series of (a) RH and T, (b) WS and WD, (c) $PM_{2.5}$, and (d) CO. Sample types of cloud ~~droplets (CD~~droplet residuals (CDR), interstitial aerosol particles (INT), and cloud-free aerosol particles (CF) are shaded as blue, purple, and gray, respectively.

Each CE's sampling period is divided into three stages (pre-cloud, in-cloud, and post-cloud) to compare OA characteristics. The in-cloud stage corresponds to the sample types of ~~CD~~CDR and INT, whereas both the pre-cloud and post-cloud stages correspond to the sample type of CF ($PM_{2.5}$). Detailed characteristics of sample types in four CEs, such as mean chemical formula, H/C, O/C, N/C, and OSc (carbon oxidation states, 2×O/C−H/C), are shown in Table 1, and division of stages is shown in Fig. S1.

A total of 2084 molecular formulas of OA were identified in the campaign. Mean formula of ~~CD~~CDR was $C_{9.95–12.92}H_{14.53–21.78}O_{5.15–6.02}N_{0.32–0.42}S_{0–0.01}Si_{0–1.29}$ for CE1–CE4. Compared with pre-cloud aerosols with formula $C_{8.17–10.57}H_{12.99–16.14}O_{4.98–5.64}N_{0.12–0.30}S_{0–0.01}Si_{0–0.24}$, ~~CD~~CDR exhibited increased numbers of carbon, hydrogen, oxygen, and nitrogen atoms, with the differences being statistically significant ($p< 0.05$) (Table S2). These molecular formulas were classified into eight classes, that is, CHO (only C, H, O atoms are contained in the chemical formula, hereafter), CHON, CHONS, CHOS, CHN, CHS, CHNS, and CHOSi. Since the composition of OA varied in different CEs, the fractions of these OA classes are discussed for each CE in Sect. 3.2. The O/C ratio was generally lower in ~~CD~~CDR (0.45–0.66) than in pre-cloud aerosols, INT, and post-cloud aerosols in 4 CEs. The O/C ratio in ~~CD~~CDR is comparable to those reported for fog water (0.52–0.68), aqSOA (0.61–0.84), and oxygenated OA (0.44–0.83) by Gilardoni et al. (2016). In general, O/C of ~~CD~~CDR in this study is comparable to that of fog (0.58–0.8) in the Po Valley in Brege et al. (2018), while H/C of ~~CD~~CDR (1.50–1.87) is higher than that of fog (1.29–1.37) in that study. Furthermore, ~~CD~~CDR showed elevated N/C (0.033–0.045) relative to other sample types, while its OSc value (−0.83 to −0.25) is generally lower than in other sample types.

Table 1. Mean molecular formulas and elemental parameters (H/C, O/C, N/C, and OSc; mean ± standard deviation) of OA for CE1–CE4 in pre-cloud aerosols, ~~CD~~CDR, INT, and post-cloud aerosols.

		Pre-cloud aerosols	~~CD~~CDR	INT	Post-cloud aerosols
CE1	Formula	$C_{8.72}H_{13.81}O_{5.64}N_{0.20}S_{0}Si_{0.24}$	$C_{10.45}H_{17.25}O_{6.02}N_{0.32}S_{0}Si_{0.69}$	$C_{8.99}H_{14.21}O_{5.68}N_{0.26}S_{0}Si_{0.23}$	$C_{8.86}H_{14.45}O_{5.71}N_{0.22}S_{0}Si_{0.40}$
	H/C	1.61±0.04	1.64±0.11	1.61±0.04	1.61±0.04
	O/C	0.71±0.02	0.66±0.03	0.69±0.02	0.70±0.02
	N/C	0.022±0.004	0.033±0.008	0.028±0.005	0.025±0.006
	OSc	-0.19±0.06	-0.33±0.14	-0.22±0.06	-0.20±0.06
CE2	Formula	$C_{8.33}H_{13.72}O_{4.98}N_{0.28}S_{0.01}Si_{0.16}$	$C_{10.13}H_{19.51}O_{5.44}N_{0.39}S_{0.01}Si_{1.29}$	$C_{8.52}H_{14.19}O_{4.92}N_{0.33}S_{0.01}Si_{0.20}$	$C_{11.12}H_{21.10}O_{6.26}N_{0.33}S_{0.01}Si_{1.52}$
	H/C	1.70±0.03	1.87±0.15	1.72±0.04	1.78±0.13
	O/C	0.63±0.01	0.58±0.03	0.61±0.02	0.61±0.02
	N/C	0.037±0.004	0.045±0.01	0.042±0.009	0.031±0.006
	OSc	-0.43±0.04	-0.71±0.19	-0.50±0.08	-0.56±0.15
CE3	Formula	$C_{10.57}H_{16.14}O_{5.08}N_{0.30}S_{0.01}Si_{0.02}$	$C_{12.92}H_{21.78}O_{5.15}N_{0.42}S_{0.01}Si_{0.87}$	$C_{10.42}H_{16.21}O_{5.09}N_{0.27}S_{0.004}Si_{0.11}$	$C_{10.51}H_{16.18}O_{5.11}N_{0.27}S_{0.01}Si_{0.07}$
	H/C	1.57±0.01	1.73±0.08	1.59±0.01	1.58±0.01
	O/C	0.55±0.008	0.45±0.03	0.55±0.005	0.55±0.005
	N/C	0.033±0.002	0.040±0.007	0.028±0.002	0.029±0.002
	OSc	-0.48±0.02	-0.83±0.12	-0.49±0.02	-0.47±0.02
CE4	Formula	$C_{8.17}H_{12.99}O_{5.29}N_{0.12}S_{0.004}Si_{0}$	$C_{9.95}H_{14.53}O_{5.68}N_{0.32}S_{0.01}Si_{0}$	$C_{8.94}H_{13.36}O_{5.52}N_{0.20}S_{0.004}Si_{0}$	$C_{8.77}H_{13.20}O_{5.52}N_{0.18}S_{0.004}Si_{0}$
	H/C	1.65±0.02	1.50±0.04	1.52±0.02	1.52±0.01
	O/C	0.69±0.01	0.62±0.02	0.66±0.008	0.67±0.01
	N/C	0.014±0.005	0.034±0.01	0.021±0.005	0.019±0.003
	OSc	-0.28±0.04	-0.25±0.07	-0.20±0.02	-0.18±0.02

3.2 Comparison of cloud episodes

The fractions of three OA classes which are CHO, CHON, and Others (including CHONS, CHOS, CHN, CHS, CHNS, and CHOSi) exhibited general similarities across the four CEs, as shown in Fig. 3. In all sample types (pre-cloud aerosols, ~~CD~~CDR, INT, and post-cloud aerosols) of the four CEs, CHO dominated OA composition, accounting for > 50 % of signal intensity of OA (54.6 %–85.7 % from CE1 to CE4), followed by CHON (14.0 %–33.2 %) and Others (lower than 18.7 %). The Others class, predominantly CHOSi, accounted for 0.5 %–18.7 % in ~~CD~~CDR, exceeding the fractions in other sample types~~, and is further discussed at the level of individual compounds below.~~. In most cloud episodes, ~~CD~~CDR showed the lowest CHO fraction (54.8 %–70.7 %) and the highest CHON fraction (26.6 %–33.2 %) among the four sample types. In CE2, the higher CHON (29.4 %) and lower CHO (54.6 %) in post-cloud aerosols than in other sample types are attributable to air mass changes during the long-time interval between post-cloud and others (shown in Fig. 2 and Fig. S1), as indicated by elevated CO concentration. CHON compounds have been detected in cloud and fog water in numerous studies (LeClair et al., 2012; Sun et al., 2024a; Sun et al., 2021; Sun et al., 2024b). Higher CHON fraction (59.0 %–63.5 %) in fog water than aerosol particles (51.2 %–51.5 %) was reported previously in Sun et al. (2024a), which is in agreement with the results in this study. In addition, the greater number of CHON compounds in ~~CD~~CDR compared with CF underscores the role of cloud processing

in enhancing CHON, as reflected in the number fraction rather than the intensity fraction (Boone et al., 2015; Liu et al., 2023b). The fraction of CHON (19.7 %–26.3 %) in INT was lower than in ~~CD~~CDR (26.6 %–33.2 %) and higher than in pre-cloud aerosols (14.0 %–23.1 %) in CE1, CE2, and CE4. However, in CE3, the slightly lower CHON fraction in INT compared to pre-cloud aerosols may be due to turbulence in clouds resulting from the short duration time of the cloud (several minutes). ~~Higher~~A higher relative abundance of CHON in ~~CD~~CDR (43.6 %–65.3 %) compared to INT (31.8 %–51.0 %) has been observed at Tianjing Mountain in southern China (Sun et al., 2021), consistent with our results. The higher CHON fraction in ~~CD~~CDR than in pre-cloud aerosols suggests that cloud processing promoted CHON formation. Higher CHON in INT compared to pre-cloud aerosols indicates that although not activated into cloud droplets, high RH experienced by INT (close to 100 %) and corresponding high aerosol water content could still promote CHON formation in INT, consistent with the elevated N/C ratio of aqSOA of aerosol particles under high RH conditions (Zhao et al., 2019). We would like to note that it is assumed that different classes of compounds have similar sensitivity in EESI-ToF-MS.

Among the CHON class, the compounds enriched in ~~CD~~CDR, such as $C_{8-12}H_{11-19}NO_{5-8}$ and $C_{14-16}H_{21-27}NO_{4-9}$, with an O/N ratio of ≥3 (71 %–88 % for CE1, CE3, and CE4, and 17% for CE2), suggesting that they are likely organonitrates, amino acids, or N-containing heterocyclic compounds. At the Shanghuang site, emissions of monoterpenes and sesquiterpenes are abundant (Zhang et al., 2024). Consequently, $C_{10}H_{15}NO_x$ and $C_{10}H_{17}NO_x$ may be formed via hydroxyl oxidation of monoterpene in the presence of NO (Shen et al., 2022) or NO_3 oxidation (Shen et al., 2021; Guo et al., 2022) and dissolve in the aqueous phase, whereas $C_{15}H_{23}NO_x$ and $C_{15}H_{25}NO_x$ may originate from similar reactions involving sesquiterpenes. Additionally, precursors could form organonitrates through aqueous reactions, e.g., with NO_3 radicals (Ng et al., 2017), or involving NO_3^- (Sun et al., 2024b; Huang et al., 2023; Barber et al., 2024). These reactions can occur at night or even during the day under reduced light conditions in clouds. This finding contrasts with the observation at Mt. Tai, where, despite the higher number of CHON compounds in ~~CD~~CDR relative to CF, a larger fraction contained reduced nitrogen groups (O/N <3) (Liu et al., 2023b). Such disparity may arise from differences in precursors between the two sampling sites. Additional information, such as the gas-phase CHON composition and concentration, is required to further elucidate the formation mechanisms of these compounds.

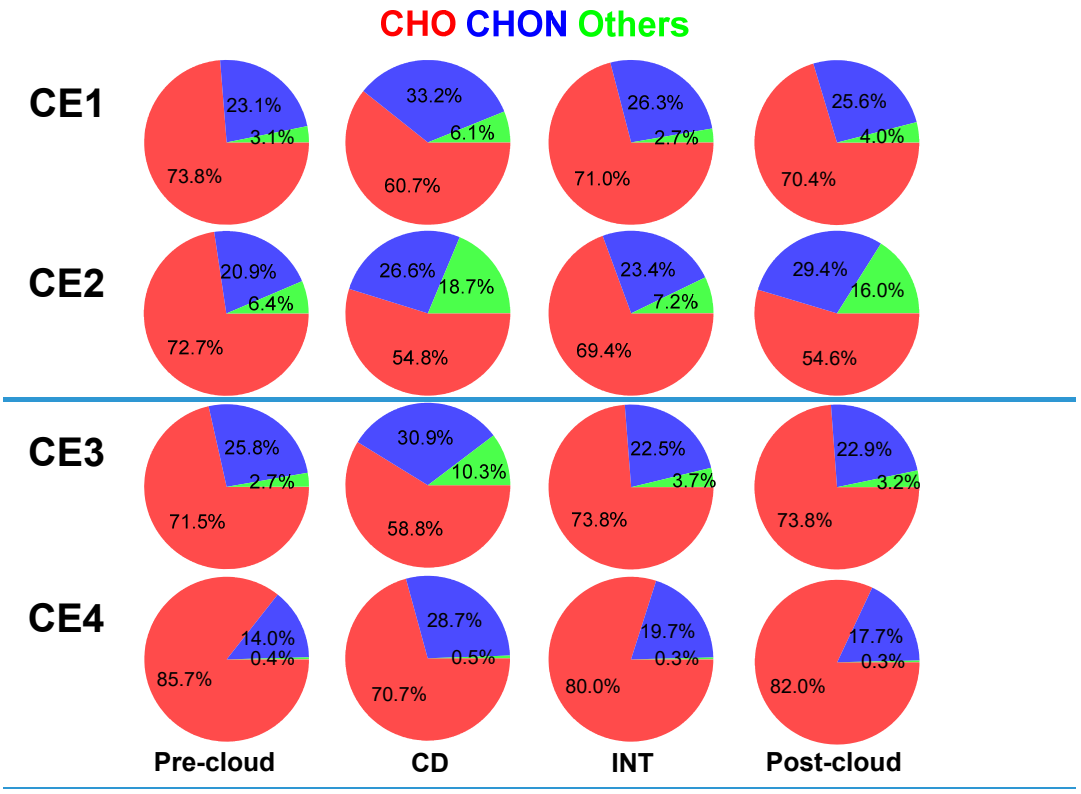

225

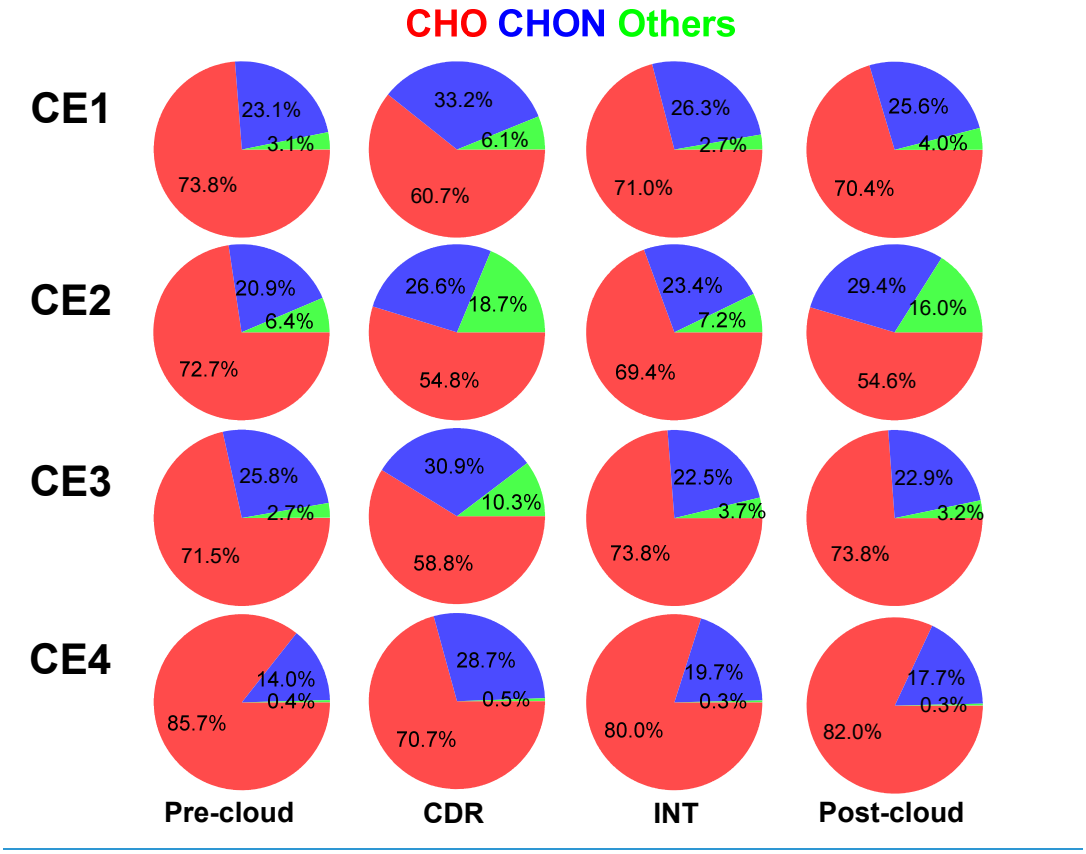

Figure 3. Fractions of three classes of OA, namely CHO, CHON, and Others (including CHONS, CHOS, CHN, CHS, CHNS, and CHOSi) in pre-cloud aerosols, ~~CD~~CDR, INT, and post-cloud aerosols in CE1, CE2, CE3, and CE4.

The molecular composition characteristics of OA in four CEs exhibit similar patterns, presented as carbon number

230 distribution colored according to the numbers of oxygen and nitrogen; therefore, only CE2 and CE3 are shown in Fig. 4 (CE1 and CE4 in Fig. S3). In each CE, comparison is carried out between ~~CD~~CDR and CF which was the closest to ~~CD~~CDR

temporally: for CE1–3, ~~CD~~CDR is compared with pre-cloud aerosols, while CE4 is compared with post-cloud aerosols, as shown in Fig. S1. In ~~CD~~CDR, the carbon number of OA ranged from 2 to 28 (CE2: 3–27; CE3: 2–28), and the oxygen number ranged from 0 to 10 in CE2 and 0 to 15 in CE3. Comparing with OA in CF, OA in ~~CD~~CDR contained a higher fraction of compounds with $n_C > 10$ as well as elevated n_O (CE2: n_O=7–10; CE3: n_O=6–15).

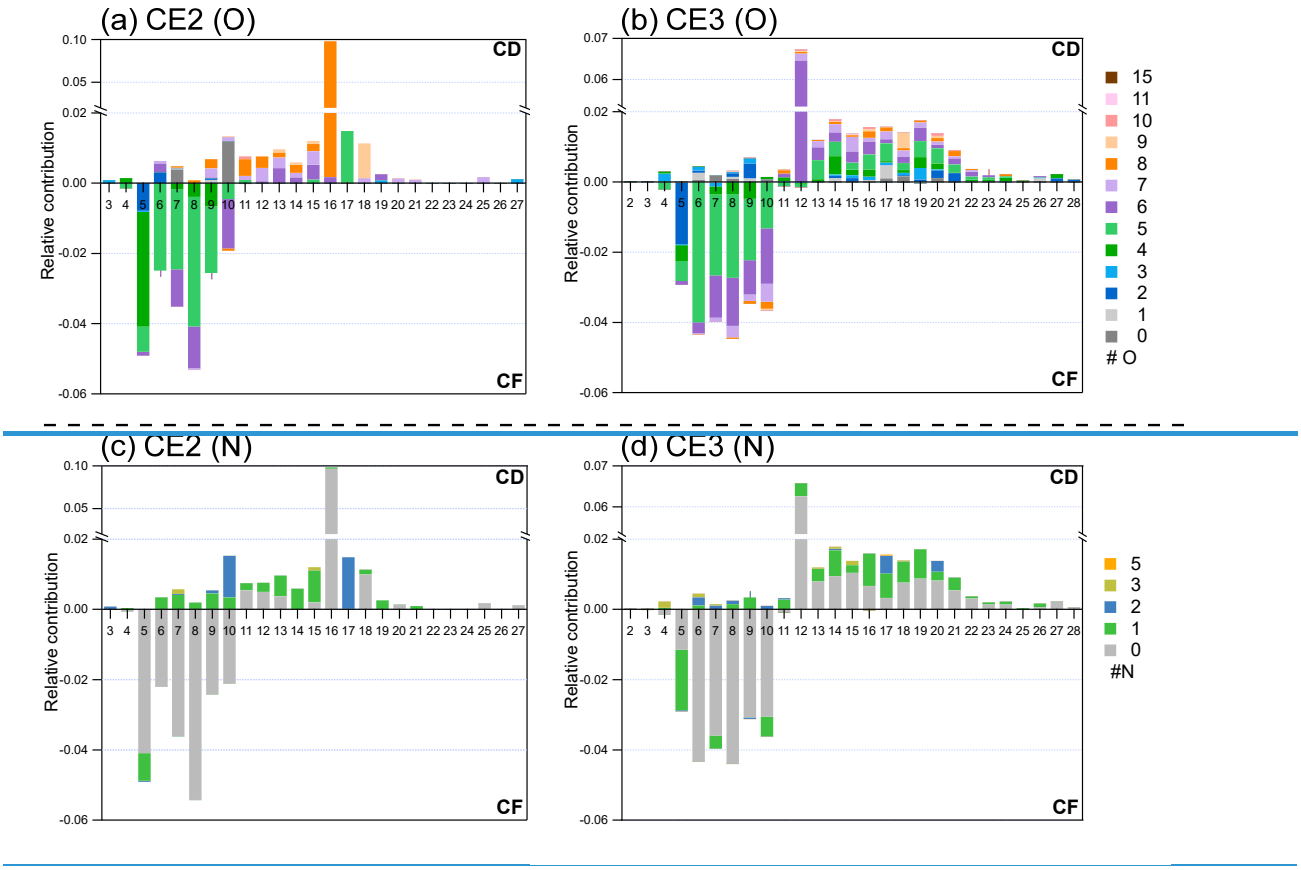

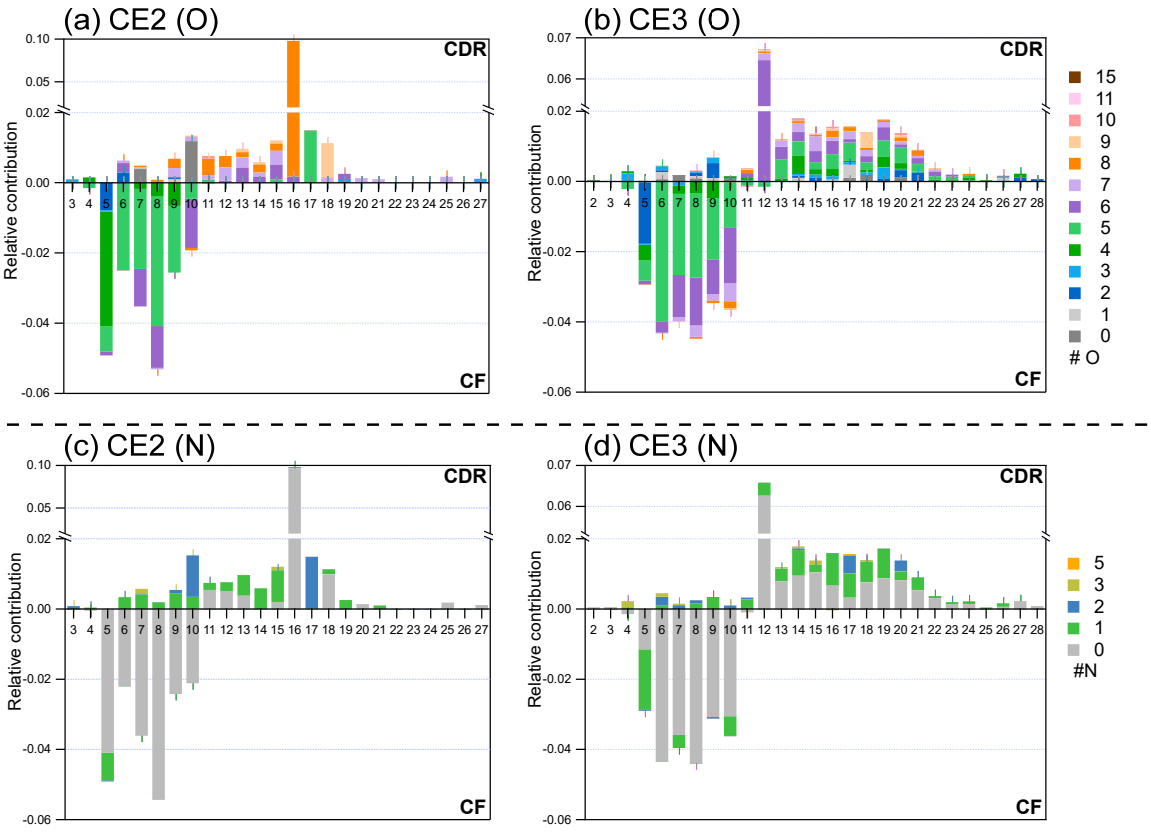

Figure 4. Detailed relative contribution of OA. The average carbon number distribution of differences between ~~CD~~CDR and CF are colored by oxygen number of (a) CE2, (b) CE3; and nitrogen number of (c) CE2, (d) CE3. Positive value stands for significant molecular characteristics of ~~CD~~CDR, and negative value stands for that of CF. Fractions of compounds are normalized to sum of signals of all organics in ~~CD~~CDR and CF, respectively.

The nitrogen number (n_N) distributions relative to n_C exhibit similar patterns in all CEs. In CE2, the n_N of N-containing OA is distributed from 0 to 3, and from 0 to 5 in CE3. The n_C of N-containing OA ranged from 3 to 21 in CE2 and 4 to 27 in CE3. Compared with CF, ~~CD~~CDR contained a larger fraction of N-containing OA, especially those with n_N=1–3 and higher n_C. Collectively, compounds in ~~CD~~CDR had more n_C, n_O, and n_N than those in CF. The molecular characteristic of higher n_C is likely attributed to accretion reactions such as oligomerization (Yu et al., 2016; Fenselau et al., 2025). This finding is consistent with several laboratory studies of aqSOA formation. For instance, enriched high-molecular-weight compounds (HMWC) in aqSOA were reported in the bulk phase experiments of methylglyoxal and glyoxal under cloud-relevant conditions (Tan et al., 2009; Altieri et al., 2008). And aqSOA from in-cloud simulation using a wetted-wall flow reactor has more highly oxygenated and carbon-containing compounds than gasSOA simulated by an oxidation flow reactor (OFR) from the same biomass burning samples (Wang et al., 2024b). Experiments in the bulk phase and the wetted-wall flow reactor which better represents atmospheric aqueous conditions, indicate that accretion reactions could be prevalent in cloud droplets. Field observations in the Arctic also show potential evidence of accretion reactions, with compounds of longer carbon chains

enriched in ~~CD~~CDR relative to CF (Pasquier et al., 2022), hinting at the possible importance of accretion reactions. Notably, this study provides direct molecular-level evidence for the contribution of accretion reactions during cloud processing of OA.

To investigate OA processing when the cloud episode changed from CF to ~~CD~~CDR, CH_2-based Kendrick mass defect (KMD) plots for CE2 and CE3 are analyzed (Fig. 5). The chemical formulas of compounds with a larger fraction in ~~CD~~CDR than CF in four CEs are listed in Table S3. Several series of compounds in CE2 and CE3 exhibit sequential increase in CH_2 groups, such as $C_{10}H_{15}NO_6(CH_2)_n$, $C_8H_{11}NO_7(CH_2)_n$, $C_4H_6O_5(CH_2)_n$, $C_5H_6O_5(CH_2)_n$, $C_5H_6O_6(CH_2)_n$, $C_7H_8O_6(CH_2)_n$. Specifically, numerous CHON compounds were present at higher fractions in ~~CD~~CDR, with some labeled by formulas such as series of $C_6H_9NO_7(CH_2)_{0–4}$, $C_7H_{11}NO_6(CH_2)_{0,2,3}$, $C_8H_{11}NO_7(CH_2)_{0–5,7}$, and $C_{12}H_{17}NO_8(CH_2)_{0–3}$ in CE2 and series of $C_7H_9NO_4(CH_2)_{0,3,7,9}$, $C_8H_{11}NO_7(CH_2)_{0–3,6,8–9,12}$, $C_{10}H_{15}NO_6(CH_2)_{0–4,6}$, $C_{12}H_{19}NO_5(CH_2)_{0,2–3}$ in CE3. This result is in agreement with the higher fraction of total CHON compounds in ~~CD~~CDR compared with CF, as discussed above. The observed CH_2-based homologous series likely reflects carbon-chain growth through aqueous accretion reactions. Possible formation pathways include peroxy radical (RO_2) addition, aldol condensation, hydroxyl-carbonyl addition (hemiacetal/acetal formation), and esterification involving precursors (Tilgner et al., 2021; Mayhew et al., 2025), which warrant further investigation. For most homologues, ~~CD~~CDR contained higher fractions of larger compounds (with more CH_2 groups) than CF, while lower fractions of smaller compounds. As detailed above, it is likely that cloud processing enhanced accretion reactions by extending the length of the carbon chain, which further highlights the importance of accretion reactions of organics in cloud droplets. In CF, CHO had a larger fraction than CHON; for example, CHO compounds such as $C_5H_6O_6(CH_2)_n$, $C_6H_{10}O_6(CH_2)_n$, and $C_5H_6O_5(CH_2)_n$ were more abundant. The pattern of adding CH_2 groups in cloud processing is similar in all CEs. However, the KMD plots based on O show that compounds in CE2 and CE3 did not exhibit a clear pattern with a sequential increase in O (Fig. S4). The dominant pattern of CH_2 addition, rather than O addition, suggests that sequential OH addition or auto-oxidation was not prevalent in cloud processing. In terms of the increments of CH_2 and O, CH_2 displays a wider growth trend (0–7) among all series, whereas O shows a narrower increase, confined to a range of 0 to 3. Consequently, results of KMD plots suggest that as cloud processing proceeded, n_C of OA increases, while the increase in n_O is lower than the n_C, agreeing with the lower O/C ratio in ~~CD~~CDR than that in CF. The possible reason is that aqueous processing is more significant in accretion (enhancing n_C) than oxygenation (enhancing n_O).

Furthermore, although oligomer formation involving subunits such as $C_2H_2O_3$ (Lim et al., 2010) and $C_3H_4O_2$ (Cook et al., 2017; Altieri et al., 2008; Tan et al., 2009) has been reported, compounds in CE of this study such as CE2 and CE3 did not seem to show clear sequential increases in these subunits (Fig. S5). This may be attributed to differences in precursors and formation mechanisms during cloud processing between the Shanghuang site and other observations and laboratory studies.

In addition, some siloxane compounds showed higher fractions in ~~CD~~CDR than in CF. The reason for the higher fraction of siloxane warrants further study.

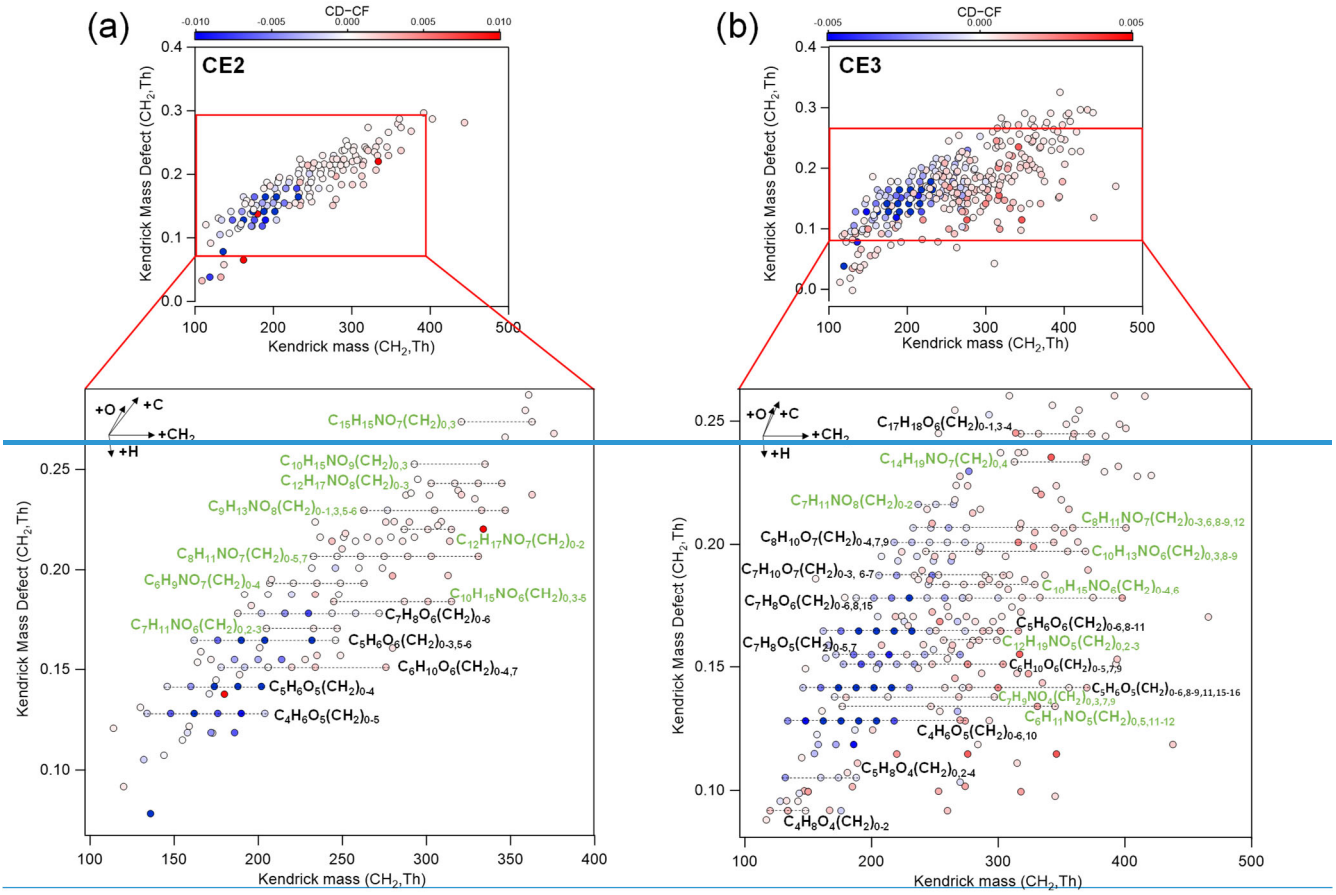

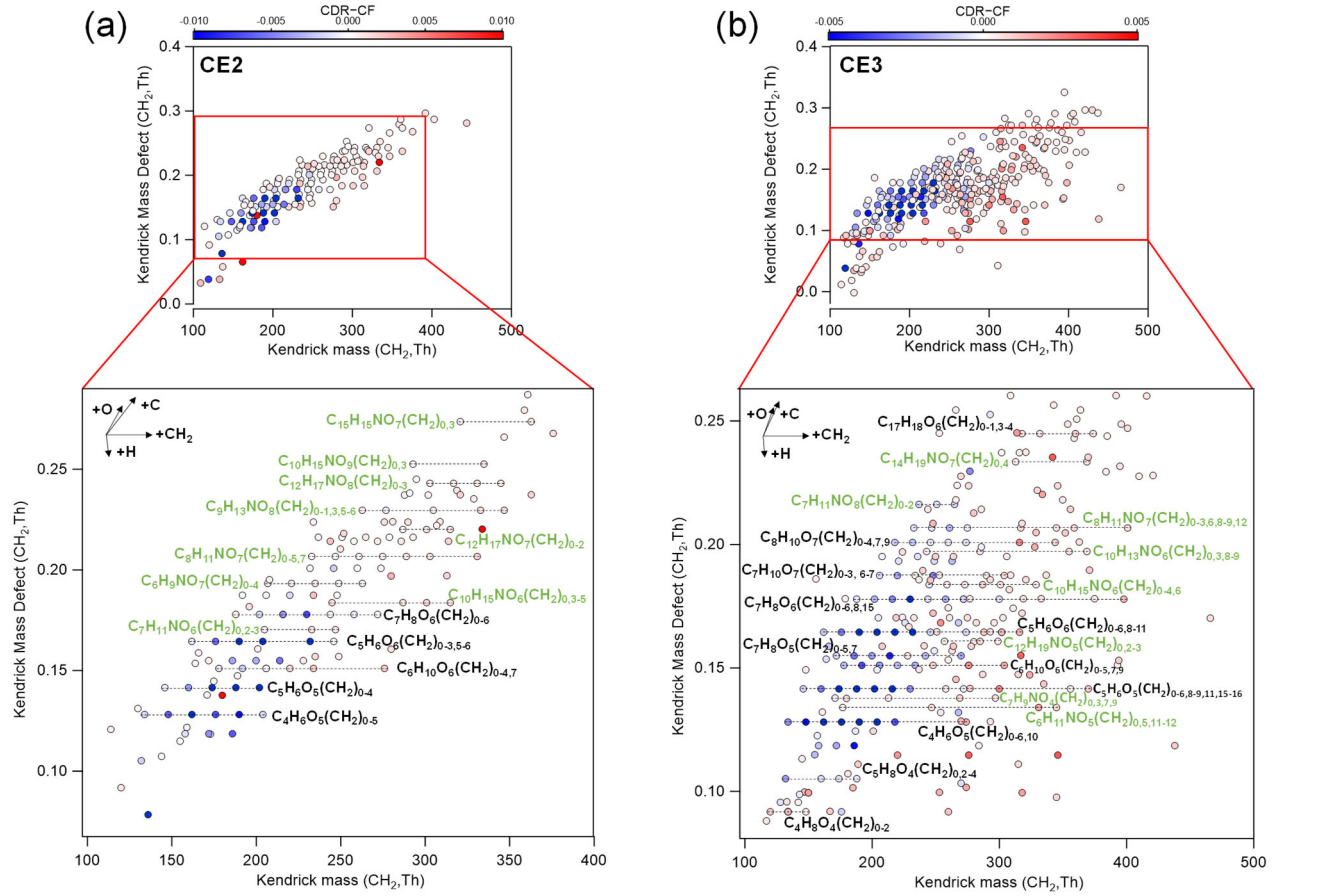

Figure 5. Kendrick mass defect plots based on CH_2 of compounds in (a) CE2 and (b) CE3. Data points are color-coded by differences in fractions of compounds between ~~CD~~CDR and CF. Fractions of compounds are normalized to the sum of signals of all organics in ~~CD~~CDR and CF, respectively. Note that, for conciseness, data points in CE3 with normalized signal difference between −0.0003 and 0.0003 (appearing nearly white) are not shown here. Siloxane compounds are not shown here for clarity.

3.3 Characteristic compounds in cloud processing and formation mechanisms

We identified ~~aqSOA tracers~~ enriched OA compounds in cloud ~~droplets~~droplet residuals by comparing the intensity fractions of all compounds between ~~CD~~CDR and CF using a *t*-test at a significant level of 0.05. A total of 144, 421, 274, and 537 organic compounds in CE1, CE2, CE3, and CE4, respectively, passed the *t*-test. Among these compounds, 39 organic compounds in ~~CD~~CDR were significantly enriched in three or four CEs, as shown in Table 2. Two were consistently significant in ~~CD~~CDR across all four CEs: $C_{14}H_{42}O_7Si_7$ and $C_9H_{22}N_2O_4$. Furthermore, sulfate compounds were enriched in ~~CD~~CDR compared with CF in three CEs, of which time series is shown in Fig. S6. Sulfate is a well-established tracer for aqueous-phase processing, and its elevated concentration in cloud droplets and fog has been widely reported (Dadashazar et al., 2022; Brege et al., 2018; Kim et al., 2019), which further enhances the potential of identifying the enriched OA compounds as aqSOA tracers formed via cloud processing. The number of CHO, CHON, CHN, and CHOSi compounds is 15, 19, 2, and 3, respectively. The majority of the enriched OA compounds exhibit carbon numbers greater than nine, which is also an indication of accretion reactions in cloud droplets. Most of these enriched OA compounds have not been reported in previous literature (Cook et al., 2017; Bianco et al., 2019; Tong et al., 2021; Sun et al., 2024b).

Table 2. Thirty-nine enriched OA compounds observed in ~~CD~~CDR of three or four CEs. These OA compounds are classified into four classes: CHO, CHON, CHN, and CHOSi.

CHO	CHON	CHN	CHOSi
$C_6H_{12}O_6$	$C_4H_7NO_4$	$C_9H_{18}N_2$	$C_{12}H_{36}O_6Si_6$
$C_{10}H_{16}O_2$	$C_5H_{11}N_2O$	$C_{12}H_{23}N$	$C_{14}H_{42}O_7Si_7$
$C_{10}H_{22}O_4$	$C_9H_{22}N_2O_4$		$C_{16}H_{48}O_8Si_8$
$C_{12}H_{26}O_5$	$C_9H_{13}NO_2$		
$C_{13}H_{22}O$	$C_{10}H_{19}NO$		
$C_{13}H_{26}O_5$	$C_{10}H_{19}NO_3$		
$C_{15}H_{24}O_{14}$	$C_{11}H_{19}NO_4$		
$C_{15}H_{26}O_8$	$C_{13}H_{30}N_2O_4$		
$C_{15}H_{32}O_6$	$C_{13}H_{23}NO_3$		
$C_{16}H_{30}O_4$	$C_{14}H_{29}N_3O_3$		
$C_{20}H_{22}O_5$	$C_{14}H_{29}NO_4$		
$C_{21}H_{36}O_8$	$C_{18}H_{33}NO_5$		
$C_{23}H_{44}O_3$	$C_{18}H_{29}NO_5$		
$C_{24}H_{40}O_3$	$C_{19}H_{37}NO_3$		
$C_{30}H_{56}O_2$	$C_{20}H_{29}NO_5$		
	$C_{21}H_{41}NO_2$		
	$C_{22}H_{34}N_2O_6$		
	$C_{29}H_{51}NO_2$		
	$C_{29}H_{51}NO_6$		

Furthermore, 236 OA compounds were significantly enriched in two of four CEs, including the common aqSOA tracer, oxalic acid ($C_2H_2O_4$), previously reported in field observations and laboratory studies (Rogers et al., 2025; Ervens et al., 2011). The compound $C_2O_4Na_3^+$ is identified as oxalic acid, of which the hydrogen atoms in the carboxylic functional group (-COOH) are substituted by Na^+ (Surdu et al., 2024). The oxalic acid signal was exclusively observed during ~~CD~~CDR, whereas it remained weak and noisy in CF and INT, as shown in Fig. 6. The oxalic acid signal was significantly enhanced only in CE2 and CE4, rather than in all CEs, which may be related to larger inhomogeneity within clouds due to strong turbulence. Meanwhile, the $C_6H_{12}O_6$ signal was as low as the detection limit in CF; however, it increased gradually when ~~CD~~CDR began. $C_6H_{12}O_6$ in aqueous formation was reported in a laboratory study and may be produced from the aqueous reaction of formaldehyde or acetaldehyde (Li et al., 2011). Therefore, it is reasonable to classify $C_6H_{12}O_6$ as a tracer of aqSOA.

Notably, N-containing compounds were significant in ~~CD~~CDR, such as $C_{12}H_{23}N$ and $C_7H_{12}N_2$ (shown in Fig. 6). $C_{12}H_{23}N$ was reported to be emitted from primary sources including vehicle emissions (Thomas et al., 2025) and agricultural residue burning (Lin et al., 2012), whereas $C_7H_{12}N_2$ (enriched in CE2) has been observed in emissions from traditional biomass fuel burning and agricultural residue burning (Fleming et al., 2018; Wang et al., 2017; Lin et al., 2012; Hao et al., 2025). $C_{12}H_{23}N$ and $C_7H_{12}N_2$ may be formed in aerosol phase and undergo uptake into cloud droplets. These compounds could also be heterocyclic compounds containing imine or amine functional groups, potentially resulting from secondary formation in the aqueous phase (Zhao et al., 2015; Li et al., 2023). In addition, $C_{12}H_{23}N$ may be a compound with a pyrrole structure. Pyrrole-derived SOA may contribute to brown carbon chromophore and influence radiative forcing (Chen et al., 2024). $C_7H_{12}N_2$ is likely 1-butylimidazole, a derivative of imidazole, reported in reactions of methylglyoxal and amines in cloud simulation in De Haan et al. (2011). Moreover, imidazole has been reported as a type of brown carbon influencing regional radiative forcing (Kim et al., 2019; Lian et al., 2020; Gan et al., 2024) and may contribute to reactive oxygenated species, potentially relating to adverse health effects (Dou et al., 2015). The enhanced concentration of N-containing compounds in ~~cloud droplets~~CDR could therefore have significant atmospheric implications and warrants further investigation.

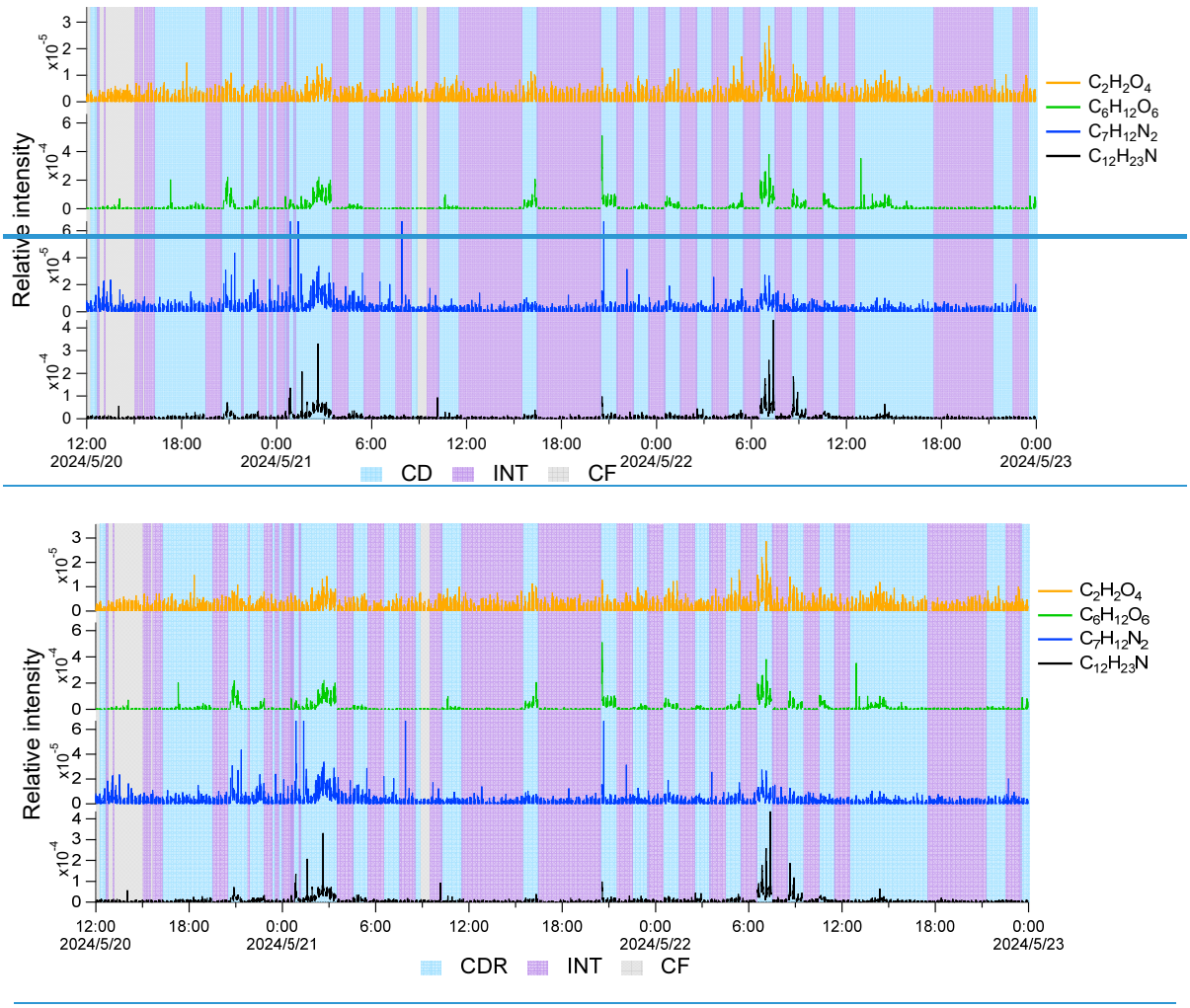

335 **Figure 6. Typical time series of compounds: carboxylic acid ($C_2H_2O_4$), $C_6H_{12}O_6$, N-containing substances including $C_7H_{12}N_2$ and $C_{12}H_{23}N$, in a cloud episode. ~~CD~~CDR, INT, and CF are shaded as blue, purple, and gray, respectively. Gaps in the time series represent EESI-ToF-MS background measurement periods, which are not shown.**

3.4 Dynamic variation of OA in clouds

340 Relatively stable T, WS, and CO concentration in a typical 3-day cloud indicate that the cloud was stable and primary emission sources remained largely constant throughout the cloud episode. The time series of CHO, CHON, and Others are shown in Fig. 7. CHO and CHON were the major constituents for most of the episode, whereas Others was the lowest. The O/N ratio was generally lower in ~~CD~~CDR than in INT, while the ratio of O/C and N/C varied irregularly in ~~CD~~CDR and INT. Although the time resolution of our measurement (~20 s) is enough to capture the evolution of a compound in clouds, either 345 in ~~CD~~CDR or INT, there is no clear trend in the time series of the compounds, either from the fractions of OA classes or elemental ratios during the sample types of ~~CD~~CDR or INT. This phenomenon is likely due to the dynamic characteristics of clouds, in which turbulence and chemical processes continuously induce rapid changes in organic compounds, resulting in no gradual trends in their concentrations.

From the perspective of the molecular composition, the relative intensities of representative compounds in cloud episodes exhibited frequent and pronounced fluctuations during individual ~~CD~~CDR periods, as shown in Fig. 6. Even within a 1-h ~~CD~~CDR, the signal of compounds increased and decreased irregularly, likely due to turbulence. Consequently, it is difficult to track and capture information on the chemical transformation of OA in clouds. Most previous comparisons of the chemical composition of cloud droplets with cloud-free aerosol particles or interstitial aerosol particles are based on long sampling (hours to a day) and offline analysis (Sun et al., 2021; Liu et al., 2023b). Based on the findings in this study, the results obtained using methods with low time resolution may be subject to uncertainties due to the dynamic nature of clouds.

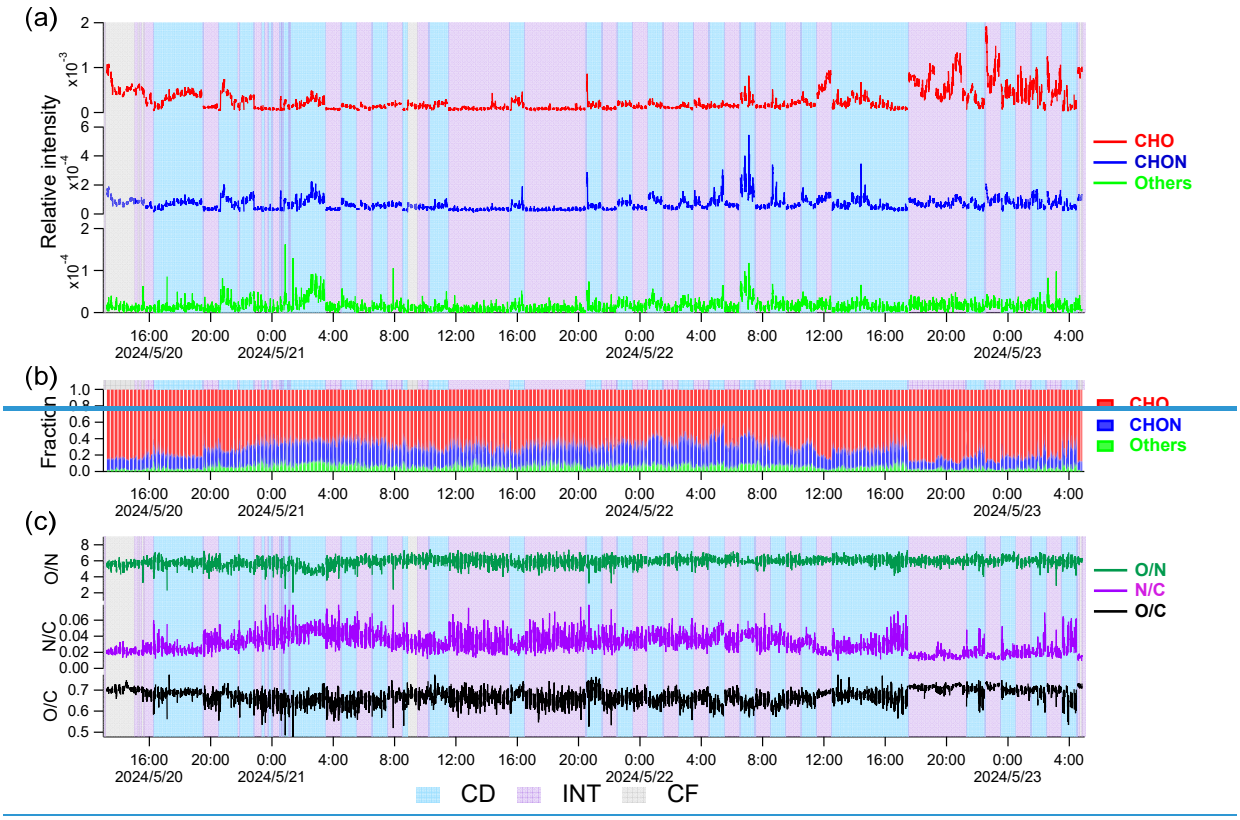

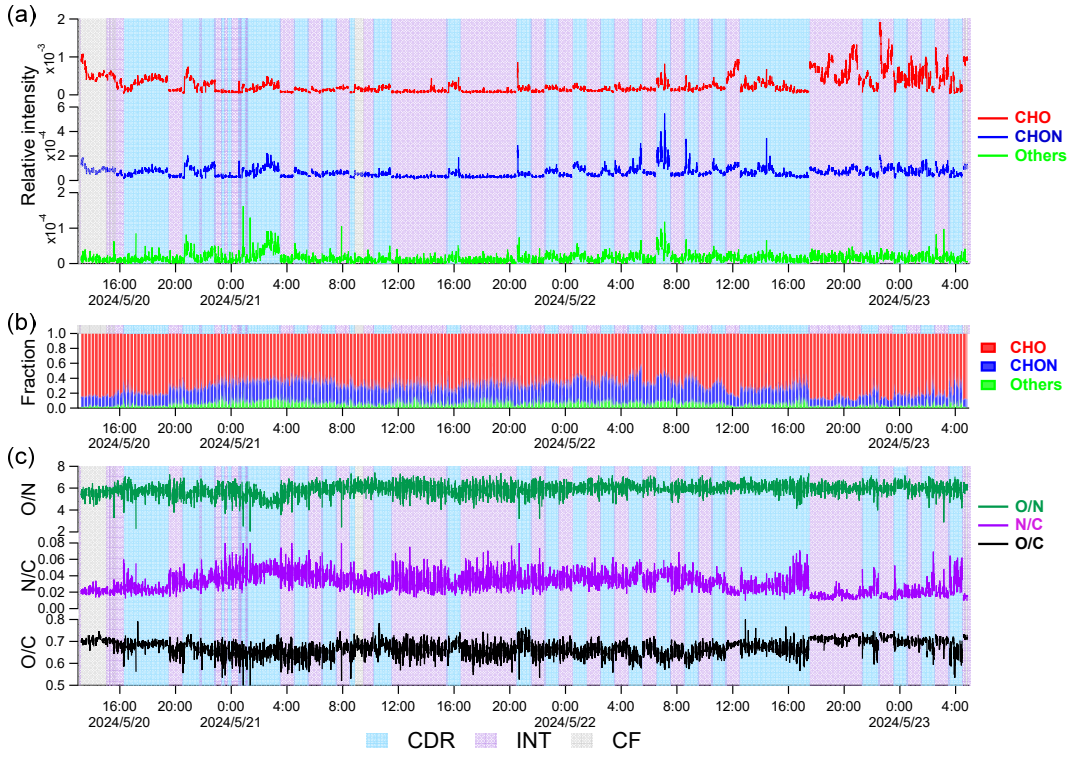

Figure 7. Time series of three classes of organic compounds (CHO, CHON, and Others) in a long cloud. (a) relative intensity, (b) fraction in OA, (c) O/N, N/C, and O/C ratio of OA. ~~CD~~CDR, INT, and CF are shaded in blue, purple, and gray, respectively. Gaps in the time series represent EESI-ToF-MS background measurement periods, which are not shown.

4 Conclusions and implications

AqSOA molecular composition and processing in cloud episodes were studied using online molecular information obtained by EESI-ToF-MS at a high-mountain site in China. Cloud processing substantially influences OA composition, resulting in large differences among distinct cloud episodes. Organics in cloud ~~droplets~~droplet residuals had an average molecular formula $C_{9.95–12.92}H_{14.53–21.78}O_{5.15–6.02}N_{0.32–0.42}S_{0–0.01}Si_{0–1.29}$ for the selected four cloud episodes. CHO compounds contributed predominantly to OA in cloud ~~droplets.~~droplet residuals. CHON was enhanced markedly in cloud ~~droplets~~droplet residuals compared with cloud-free aerosol particles and interstitial aerosol particles in most cloud episodes. The majority of CHON compounds were likely organonitrates, highlighting the enrichment of organonitrates compounds in cloud processing. OA in cloud ~~droplets~~droplet residuals contained higher numbers of C, O, and N atoms, exhibited a CH_2-based homologous series, and showed an enrichment of higher-molecular-weight compounds compared with ~~adjacent cloud-free~~ aerosol particles sampled under the temporally closest cloud-free conditions, collectively highlighting the importance of accretion reactions in cloud processing of OA at the molecular level. We identified several compounds significantly enriched in cloud ~~droplets~~droplet residuals, including typical aqSOA tracers such as oxalic acid. The new aqSOA tracers, such as $C_6H_{12}O_6$ and $C_9H_{22}N_2O_4$, could help future studies identify cloud processing aqSOA.

This study provides direct molecular-level evidence for the contribution of accretion reactions during cloud processing of OA. Although previous cloud observations using FT-ICR-MS reported the presence of oligomers in cloud samples, these studies could not distinguish whether such compounds originated from cloud processing or aqueous aerosols, as no concomitant aerosol samples were collected for comparison (Zhao et al., 2013; Cook et al., 2017). By directly comparing OA composition in cloud ~~droplets~~droplet residuals with that in cloud-free aerosol particles, our results clearly demonstrate that accretion reactions occur within cloud droplets. It has been assumed that HMWC are predominantly formed in aerosol liquid water rather than cloud water, owing to the lower reaction rates of accretion reactions in the more dilute cloud-water environment (Ervens et al., 2011). In contrast, our study provides direct molecular-level evidence that such compounds can also be formed in cloud water, extending earlier observations by Cook et al. (2017). These findings highlight that accretion reactions should be considered when modeling aqSOA formation in clouds.

The HMWC formed via accretion reaction may have implications for the environment and climate. Due to the increase in the HMWC, accretion reactions likely reduce the volatility of organics and could potentially enhance OA mass concentration and alter the aerosol size distribution after cloud evaporation. The formation of HMWC can also modify physicochemical properties, such as lifetime, oxidation state, viscosity, and hygroscopic properties, which may further influence the cloud activation of these aerosols. In addition, the formation of N-containing compounds in cloud ~~droplets~~droplet residuals, such as organonitrates, pyrrole, and imidazole, may also affect the physicochemical properties of aqSOA, e.g., contributing to brown carbon and thus affecting regional radiative forcing.

Based on the measurement of high time resolution (~20 s), we find that the concentrations of individual organic compounds were highly dynamic in clouds, which is likely due to the turbulence in clouds. Such a highly dynamic nature in clouds poses difficulties in extracting the influence of chemical processes on individual compounds for instrumentation with low temporal resolution. Therefore, our results highlight the necessity of high time resolution measurements (< 1 h), especially online systems achieving minute-level resolution to investigate the chemical processes in clouds, considering dynamic variations of compounds in clouds due to turbulence in clouds and alterations in air masses.

It should be noted that this study provides molecular formulas only, while detailed structural information is warranted to better constrain the sources, formation mechanisms, and climate impacts of aqSOA in clouds. In addition, sources of compounds enriched in cloud ~~droplets~~droplet residuals will be investigated in future studies.

Data availability. The data used in this study are available from the corresponding authors upon request: Defeng Zhao (dfzhao@fudan.edu.cn).

Supplement.

Author contributions. DZ conceptualized the research. YJ conducted the measurements with the aid of HL, DZ, ST, SX, and CN. XiaocP and GZ conducted GCVI measurements. XiaolP conducted the meteorological measurements. WX, YZ, YS, QC and LL provided support for sampling and operation of the Shanghuang site. YJ processed data and wrote the manuscript. YJ and DZ edited the manuscript with the inputs of all authors.

Competing interests. Qi Chen is a member of the editorial board of ACP.

Financial support. This work is supported by the National Natural Science Foundation of China (No. 42575109), Shanghai Pilot Program for Basic Research-Fudan University (No. 21TQ1400100 (22TQ010)), the National Natural Science Foundation of China (No. 42330605), and "Island Atmosphere and Ecology" Category IV Peak Discipline.

Acknowledgement. The authors gratefully acknowledge the NOAA Air Resources Laboratory (ARL) for the provision of the HYSPLIT transport and dispersion model and/or READY website (https://www.ready.noaa.gov) used in this publication.

References

Altieri, K. E., Seitzinger, S. P., Carlton, A. G., Turpin, B. J., Klein, G. C., and Marshall, A. G.: Oligomers formed through in-cloud methylglyoxal reactions: Chemical composition, properties, and mechanisms investigated by ultra-high resolution FT-ICR mass spectrometry, Atmos. Environ., 42, 1476-1490, https://doi.org/10.1016/j.atmosenv.2007.11.015, 2008.

Barber, V. P., LeMar, L. N., Li, Y., Zheng, J. W., Keutsch, F. N., and Kroll, J. H.: Enhanced Organic Nitrate Formation from Peroxy Radicals in the Condensed Phase, Environ. Sci. Technol. Lett., 11, 975-980, https://doi.org/10.1021/acs.estlett.4c00473, 2024.

Bianco, A., Riva, M., Baray, J. L., Ribeiro, M., Chaumerliac, N., George, C., Bridoux, M., and Deguillaume, L.: Chemical Characterization of Cloudwater Collected at Puy de Dome by FT-ICR MS Reveals the Presence of SOA Components, ACS Earth Space Chem., 3, 2076-2087, https://doi.org/10.1021/acsearthspacechem.9b00153, 2019.

Boone, E. J., Laskin, A., Laskin, J., Wirth, C., Shepson, P. B., Stirm, B. H., and Pratt, K. A.: Aqueous Processing of Atmospheric Organic Particles in Cloud Water Collected via Aircraft Sampling, Environ. Sci. Technol., 49, 8523-8530, https://doi.org/10.1021/acs.est.5b01639, 2015.

Brege, M., Paglione, M., Gilardoni, S., Decesari, S., Facchini, M. C., and Mazzoleni, L. R.: Molecular insights on aging and aqueous-phase processing from ambient biomass burning emissions-influenced Po Valley fog and aerosol, Atmos. Chem. Phys., 18, 13197-13214, https://doi.org/10.5194/acp-18-13197-2018, 2018.

Brown, W. L., Day, D. A., Stark, H., Pagonis, D., Krechmer, J. E., Liu, X., Price, D. J., Katz, E. F., DeCarlo, P. F., Masoud, C. G., Wang, D. S., Hildebrandt Ruiz, L., Arata, C., Lunderberg, D. M., Goldstein, A. H., Farmer, D. K., Vance, M. E., and Jimenez, J. L.: Real-time organic aerosol chemical speciation in the indoor environment using extractive electrospray ionization mass spectrometry, Indoor Air, 31, 141-155, https://doi.org/10.1111/ina.12721, 2021.

Chen, K., Hamilton, C., Ries, B., Lum, M., Mayorga, R., Tian, L., Bahreini, R., Zhang, H., and Lin, Y. H.: Relative Humidity Modulates the Physicochemical Processing of Secondary Brown Carbon Formation from Nighttime Oxidation of Fura

n and Pyrrole, ACS EST Air, 1, 426-437, https://doi.org/10.1021/acsestair.4c00025, 2024.

Cook, R. D., Lin, Y. H., Peng, Z., Boone, E., Chu, R. K., Dukett, J. E., Gunsch, M. J., Zhang, W., Tolic, N., Laskin, A., and Pratt, K. A.: Biogenic, urban, and wildfire influences on the molecular composition of dissolved organic compounds in cloud water, Atmos. Chem. Phys., 17, 15167-15180, https://doi.org/10.5194/acp-17-15167-2017, 2017.

Dadashazar, H., Corral, A. F., Crosbie, E., Dmitrovic, S., Kirschler, S., McCauley, K., Moore, R., Robinson, C., Schlosser, J. S., Shook, M., Thornhill, K. L., Voigt, C., Winstead, E., Ziemba, L., and Sorooshian, A.: Organic enrichment in droplet residual particles relative to out of cloud over the northwestern Atlantic: analysis of airborne ACTIVATE data, Atmos. Chem. Phys., 22, 13897-13913, https://doi.org/10.5194/acp-22-13897-2022, 2022.

de Gouw, J. A., Middlebrook, A. M., Warneke, C., Goldan, P. D., Kuster, W. C., Roberts, J. M., Fehsenfeld, F. C., Worsnop, D. R., Canagaratna, M. R., Pszenny, A. A. P., Keene, W. C., Marchewka, M., Bertman, S. B., and Bates, T. S.: Budget of organic carbon in a polluted atmosphere: Results from the New England Air Quality Study in 2002, J. Geophys. Res.-Atmos., 110, https://doi.org/10.1029/2004jd005623, 2005.

De Haan, D. O., Hawkins, L. N., Kononenko, J. A., Turley, J. J., Corrigan, A. L., Tolbert, M. A., and Jimenez, J. L.: Formation of Nitrogen-Containing Oligomers by Methylglyoxal and Amines in Simulated Evaporating Cloud Droplets, Environ. Sci. Technol., 45, 984-991, https://doi.org/10.1021/es102933x, 2011.

Dou, J., Lin, P., Kuang, B.-Y., and Yu, J. Z.: Reactive Oxygen Species Production Mediated by Humic-like Substances in Atmospheric Aerosols: Enhancement Effects by Pyridine, Imidazole, and Their Derivatives, Environ. Sci. Technol., 49, 6457-6465, https://doi.org/10.1021/es5059378, 2015.

Duan, J., Huang, R.-J., Gu, Y., Lin, C., Zhong, H., Wang, Y., Yuan, W., Ni, H., Yang, L., Chen, Y., Worsnop, D. R., and O'Dowd, C.: The formation and evolution of secondary organic aerosol during summer in Xi'an: Aqueous phase processing in fog-rain days, Sci. Total Environ., 756, https://doi.org/10.1016/j.scitotenv.2020.144077, 2021.

Duan, J., Huang, R.-J., Gu, Y., Lin, C., Zhong, H., Xu, W., Liu, Q., You, Y., Ovadnevaite, J., Ceburnis, D., Hoffmann, T., and O'Dowd, C.: Measurement report: Large contribution of biomass burning and aqueous-phase processes to the winterime secondary organic aerosol formation in Xi'an, Northwest China, Atmos. Chem. Phys., 22, 10139-10153, https://doi.org/10.5194/acp-22-10139-2022, 2022.

Ervens, B., Turpin, B. J., and Weber, R. J.: Secondary organic aerosol formation in cloud droplets and aqueous particles (aqSOA): a review of laboratory, field and model studies, Atmos. Chem. Phys., 11, 11069-11102, https://doi.org/10.5194/acp-11-11069-2011, 2011.

Fenselau, R. Z., Alotbi, A. R., Lee, C. B., Cronin, J. S., Hill, D. R., Belitsky, J. M., and Elrod, M. J.: A New Potential Atmospheric Accretion Mechanism: Acid-Catalyzed Hetero-Michael Addition Reactions, ACS Earth Space Chem., 9, 191-200, https://doi.org/10.1021/acsearthspacechem.4c00342, 2025.

Fleming, L. T., Lin, P., Laskin, A., Laskin, J., Weltman, R., Edwards, R. D., Arora, N. K., Yadav, A., Meinardi, S., Blake, D. R., Pillarisetti, A., Smith, K. R., and Nizkorodov, S. A.: Molecular composition of particulate matter emissions from dung and brushwood burning household cookstoves in Haryana, India, Atmos. Chem. Phys., 18, 2461-2480, https://doi.org/10.5194/acp-18-2461-2018, 2018.

Fu, T.-M., Jacob, D. J., Wittrock, F., Burrows, J. P., Vrekoussis, M., and Henze, D. K.: Global budgets of atmospheric glyoxal and methylglyoxal, and implications for formation of secondary organic aerosols, J. Geophys. Res., 113, D15303, https://doi.org/10.1029/2007jd009505, 2008.

Galloway, J. N., Likens, G. E., and Edgerton, E. S.: Acid Precipitation In the Northeastern United States: pH and Acidity, Science, 194, 722-724, https://doi.org/10.1126/science.194.4266.722, 1976.

Gan, Y., Lu, X., Chen, S., Jiang, X., Yang, S., Ma, X., Li, M., Yang, F., Shi, Y., and Wang, X.: Aqueous-phase formation of N-containing secondary organic compounds affected by the ionic strength, J Environ Sci (China), 138, 88-101, https://doi.org/10.1016/j.jes.2023.03.003, 2024.

Gao, M., Zhou, S., He, Y., Zhang, G., Ma, N., Li, Y., Li, F., Yang, Y., Peng, L., Zhao, J., Bi, X., Hu, W., Sun, Y., Wang, B., and Wang, X.: In Situ Observation of Multiphase Oxidation-Driven Secondary Organic Aerosol Formation during Clou

d Processing at a Mountain Site in Southern China, Environ. Sci. Technol. Lett., 10, 573−581, https://doi.org/10.1021/acs.estlett.3c00331, 2023.

Gilardoni, S., Massoli, P., Paglione, M., Giulianelli, L., Carbone, C., Rinaldi, M., Decesari, S., Sandrini, S., Costabile, F., Gobbi, G. P., Pietrogrande, M. C., Visentin, M., Scotto, F., Fuzzi, S., and Facchini, M. C.: Direct observation of aqueous secondary organic aerosol from biomass-burning emissions, Proc. Natl. Acad. Sci. U. S. A., 113, 10013-10018, https://doi.org/10.1073/pnas.1602212113, 2016.

Graedel, T. E. and Weschler, C. J.: Chemistry Within Aqueous Atmospheric Aerosols And Raindrops, Reviews of Geophysics, 19, 505-539, https://doi.org/10.1029/RG019i004p00505, 1981.

Gramlich, Y., Siegel, K., Haslett, S. L., Freitas, G., Krejci, R., Zieger, P., and Mohr, C.: Revealing the chemical characteristics of Arctic low-level cloud residuals – in situ observations from a mountain site, Atmos. Chem. Phys., 23, 6813-6834, https://doi.org/10.5194/acp-23-6813-2023, 2023.

Guo, Y., Shen, H., Pullinen, I., Luo, H., Kang, S., Vereecken, L., Fuchs, H., Hallquist, M., Acir, I.-H., Tillmann, R., Rohrer, F., Wildt, J., Kiendler-Scharr, A., Wahner, A., Zhao, D., and Mentel, T. F.: Identification of highly oxygenated organic molecules and their role in aerosol formation in the reaction of limonene with nitrate radical, Atmos. Chem. Phys., 22, 11323-11346, https://doi.org/10.5194/acp-22-11323-2022, 2022.

Hao, Y., Strahl, J., Khare, P., Cui, T., Schneider-Beltran, K., Qi, L., Wang, D., Top, J., Surdu, M., Bhattu, D., Bhowmik, H. S., Vats, P., Rai, P., Kumar, V., Ganguly, D., Szidat, S., Uzu, G., Jaffrezo, J. L., Elazzouzi, R., Rastogi, N., Slowik, J., Haddad, I. E., Tripathi, S. N., Prevot, A. S. H., and Daellenbach, K. R.: Transported smoke from crop residue burning as the major source of organic aerosol and health risks in northern Indian cities during post-monsoon, Environ Int, 202, 109583, https://doi.org/10.1016/j.envint.2025.109583, 2025.

Herckes, P., Valsaraj, K. T., and Collett, J. L., Jr.: A review of observations of organic matter in fogs and clouds: Origin, processing and fate, Atmos. Res., 132, 434-449, https://doi.org/10.1016/j.atmosres.2013.06.005, 2013.

Huang, W., Huang, R. J., Duan, J., Lin, C., Zhong, H., Xu, W., Gu, Y., Ni, H., Chang, Y., and Wang, X.: Size-Dependent Nighttime Formation of Particulate Secondary Organic Nitrates in Urban Air, J. Geophys. Res.-Atmos., 128, https://doi.org/10.1029/2022jd038189, 2023.

Jimenez, J. L., Canagaratna, M. R., Donahue, N. M., Prevot, A. S. H., Zhang, Q., Kroll, J. H., DeCarlo, P. F., Allan, J. D., Coe, H., Ng, N. L., Aiken, A. C., Docherty, K. S., Ulbrich, I. M., Grieshop, A. P., Robinson, A. L., Duplissy, J., Smith, J. D., Wilson, K. R., Lanz, V. A., Hueglin, C., Sun, Y. L., Tian, J., Laaksonen, A., Raatikainen, T., Rautiainen, J., Vaattovaara, P., Ehn, M., Kulmala, M., Tomlinson, J. M., Collins, D. R., Cubison, M. J., Dunlea, E. J., Huffman, J. A., Onasch, T. B., Alfarra, M. R., Williams, P. I., Bower, K., Kondo, Y., Schneider, J., Drewnick, F., Borrmann, S., Weimer, S., Demerjian, K., Salcedo, D., Cottrell, L., Griffin, R., Takami, A., Miyoshi, T., Hatakeyama, S., Shimono, A., Sun, J. Y., Zhang, Y. M., Dzepina, K., Kimmel, J. R., Sueper, D., Jayne, J. T., Herndon, S. C., Trimborn, A. M., Williams, L. R., Wood, E. C., Middlebrook, A. M., Kolb, C. E., Baltensperger, U., and Worsnop, D. R.: Evolution of Organic Aerosols in the Atmosphere, Science, 326, 1525-1529, https://doi.org/10.1126/science.1180353, 2009.

Kim, H., Collier, S., Ge, X., Xu, J., Sun, Y., Jiang, W., Wang, Y., Herckes, P., and Zhang, Q.: Chemical processing of water-soluble species and formation of secondary organic aerosol in fogs, Atmos. Environ., 200, 158-166, https://doi.org/10.1016/j.atmosenv.2018.11.062, 2019.

Kumar, V., Giannoukos, S., Haslett, S. L., Tong, Y., Singh, A., Bertrand, A., Lee, C. P., Wang, D. S., Bhattu, D., Stefenelli, G., Dave, J. S., Puthussery, J. V., Qi, L., Vats, P., Rai, P., Casotto, R., Satish, R., Mishra, S., Pospisilova, V., Mohr, C., Bell, D. M., Ganguly, D., Verma, V., Rastogi, N., Baltensperger, U., Tripathi, S. N., Prévôt, A. S. H., and Slowik, J. G.: Highly time-resolved chemical speciation and source apportionment of organic aerosol components in Delhi, India, using extractive electrospray ionization mass spectrometry, Atmos. Chem. Phys., 22, 7739-7761, https://doi.org/10.5194/acp-22-7739-2022, 2022.

Lamkaddam, H., Dommen, J., Ranjithkumar, A., Gordon, H., Wehrle, G., Krechmer, J., Majluf, F., Salionov, D., Schmale, J., Bjelic, S., Carslaw, K. S., El Haddad, I., and Baltensperger, U.: Large contribution to secondary organic aerosol from i

soprene cloud chemistry, Sci. Adv., 7, eabe2952, https://doi.org/10.1126/sciadv.abe2952, 2021.

Lance, S., Zhang, J., Schwab, J. J., Casson, P., Brandt, R. E., Fitzjarrald, D. R., Schwab, M. J., Sicker, J., Lu, C. H., Chen, S. P., Yun, J., Freedman, J. M., Shrestha, B., Min, Q. L., Beauharnois, M., Crandall, B., Joseph, E., Brewer, M. J., Minder, J. R., Orlowski, D., Christiansen, A., Carlton, A. G., and Barth, M. C.: Overview of the CPOC Pilot Study at Whiteface Mountain, NY Cloud Processing of Organics within Clouds (CPOC), Bull. Amer. Meteorol. Soc., 101, E1820-E1841, https://doi.org/10.1175/bams-d-19-0022.1, 2020.

LeClair, J. P., Collett, J. L., and Mazzoleni, L. R.: Fragmentation Analysis of Water-Soluble Atmospheric Organic Matter Using Ultrahigh-Resolution FT-ICR Mass Spectrometry, Environ. Sci. Technol., 46, 4312-4322, https://doi.org/10.1021/es203509b, 2012.

Li, Y., Fu, T. M., Yu, J. Z., Yu, X., Chen, Q., Miao, R., Zhou, Y., Zhang, A., Ye, J., Yang, X., Tao, S., Liu, H., and Yao, W.: Dissecting the contributions of organic nitrogen aerosols to global atmospheric nitrogen deposition and implications for ecosystems, Natl Sci Rev, 10, nwad244, https://doi.org/10.1093/nsr/nwad244, 2023.

Li, Z., Schwier, A. N., Sareen, N., and McNeill, V. F.: Reactive processing of formaldehyde and acetaldehyde in aqueous aerosol mimics: surface tension depression and secondary organic products, Atmos. Chem. Phys., 11, 11617-11629, https://doi.org/10.5194/acp-11-11617-2011, 2011.

Lian, X., Zhang, G., Yang, Y., Lin, Q., Fu, Y., Jiang, F., Peng, L., Hu, X., Chen, D., Wang, X., Peng, P. a., Sheng, G., and Bi, X.: Evidence for the Formation of Imidazole from Carbonyls and Reduced Nitrogen Species at the Individual Particle Level in the Ambient Atmosphere, Environ. Sci. Technol. Lett., 8, 9-15, https://doi.org/10.1021/acs.estlett.0c00722, 2020.

Lim, Y. B., Tan, Y., Perri, M. J., Seitzinger, S. P., and Turpin, B. J.: Aqueous chemistry and its role in secondary organic aerosol (SOA) formation, Atmos. Chem. Phys., 10, 10521-10539, https://doi.org/10.5194/acp-10-10521-2010, 2010.

Lin, P., Rincon, A. G., Kalberer, M., and Yu, J. Z.: Elemental Composition of HULIS in the Pearl River Delta Region, China: Results Inferred from Positive and Negative Electrospray High Resolution Mass Spectrometric Data, Environ. Sci. Technol., 46, 7454-7462, https://doi.org/10.1021/es300285d, 2012.

Lin, Q., Zhang, G., Peng, L., Bi, X., Wang, X., Brechtel, F. J., Li, M., Chen, D., Peng, P. a., Sheng, G., and Zhou, Z.: In situ chemical composition measurement of individual cloud residue particles at a mountain site, southern China, Atmos. Chem. Phys., 17, 8473-8488, https://doi.org/10.5194/acp-17-8473-2017, 2017.

Liu, B., Li, Q., Sun, R., Dong, R., Wang, S., and Hao, J.: Pollution Characteristics and Factors Influencing the Reduction of Ambient $PM_{2.5}$ in Beijing from 2018 to 2020, Huanjing Kexue, 44, 2409-2420, https://doi.org/10.13227/j.hjkx.202205244, 2023a.

Liu, Z., Zhu, B., Zhu, C., Ruan, T., Li, J., Chen, H., Li, Q., Wang, X., Wang, L., Mu, Y., Collett, J., George, C., Wang, Y., Wang, X., Su, J., Yu, S., Mellouki, A., Chen, J., and Jiang, G.: Abundant nitrogenous secondary organic aerosol formation accelerated by cloud processing, iScience, 26, 108317, https://doi.org/10.1016/j.isci.2023.108317, 2023b.

Lopez-Hilfiker, F. D., Pospisilova, V., Huang, W., Kalberer, M., Mohr, C., Stefenelli, G., Thornton, J. A., Baltensperger, U., Prevot, A. S. H., and Slowik, J. G.: An extractive electrospray ionization time-of-flight mass spectrometer (EESI-TOF) for online measurement of atmospheric aerosol particles, Atmos. Meas. Tech., 12, 4867-4886, https://doi.org/10.5194/amt-12-4867-2019, 2019.

Luo, H., Guo, Y., Shen, H., Huang, D. D., Zhang, Y., and Zhao, D.: Effect of relative humidity on the molecular composition of secondary organic aerosols from α-pinene ozonolysis, Environ. Sci. - Atmospheres, 4, 519-530, https://doi.org/10.1039/d3ea00149k, 2024.

Mandariya, A. K., Gupta, T., and Tripathi, S. N.: Effect of aqueous-phase processing on the formation and evolution of organic aerosol (OA) under different stages of fog life cycles, Atmos. Environ., 206, 60-71, https://doi.org/10.1016/j.atmosenv.2019.02.047, 2019.

Mattsson, F., Neuberger, A., Heikkinen, L., Gramlich, Y., Paglione, M., Rinaldi, M., Decesari, S., Zieger, P., Riipinen, I., and Mohr, C.: Enrichment of organic nitrogen in fog residuals observed in the Italian Po Valley, Atmos. Chem. Phys., 25,

7973-7989, https://doi.org/10.5194/acp-25-7973-2025, 2025.

Mayhew, A. W., Franzon, L., Bates, K. H., Kurtén, T., Lopez-Hilfiker, F. D., Mohr, C., Rickard, A. R., Thornton, J. A., and Haskins, J. D.: The global importance of gas-phase peroxy radical accretion reactions for secondary organic aerosol loading, Atmos. Chem. Phys., 25, 17027-17046, https://doi.org/10.5194/acp-25-17027-2025, 2025.

McNeill, V. F.: Aqueous organic chemistry in the atmosphere: sources and chemical processing of organic aerosols, Environ. Sci. Technol., 49, 1237-1244, https://doi.org/10.1021/es5043707, 2015.

McNeill, V. F., Woo, J. L., Kim, D. D., Schwier, A. N., Wannell, N. J., Sumner, A. J., and Barakat, J. M.: Aqueous-Phase Secondary Organic Aerosol and Organosulfate Formation in Atmospheric Aerosols: A Modeling Study, Environ. Sci. Technol., 46, 8075-8081, https://doi.org/10.1021/es3002986, 2012.

Nault, B. A., Jo, D. S., McDonald, B. C., Campuzano-Jost, P., Day, D. A., Hu, W., Schroder, J. C., Allan, J., Blake, D. R., Canagaratna, M. R., Coe, H., Coggon, M. M., DeCarlo, P. F., Diskin, G. S., Dunmore, R., Flocke, F., Fried, A., Gilman, J. B., Gkatzelis, G., Hamilton, J. F., Hanisco, T. F., Hayes, P. L., Henze, D. K., Hodzic, A., Hopkins, J., Hu, M., Huey, L. G., Jobson, B. T., Kuster, W. C., Lewis, A., Li, M., Liao, J., Nawaz, M. O., Pollack, I. B., Peischl, J., Rappenglück, B., Reeves, C. E., Richter, D., Roberts, J. M., Ryerson, T. B., Shao, M., Sommers, J. M., Walega, J., Warneke, C., Weibring, P., Wolfe, G. M., Young, D. E., Yuan, B., Zhang, Q., de Gouw, J. A., and Jimenez, J. L.: Secondary organic aerosols from anthropogenic volatile organic compounds contribute substantially to air pollution mortality, Atmos. Chem. Phys., 21, 11201-11224, https://doi.org/10.5194/acp-21-11201-2021, 2021.

Ng, N. L., Brown, S. S., Archibald, A. T., Atlas, E., Cohen, R. C., Crowley, J. N., Day, D. A., Donahue, N. M., Fry, J. L., Fuchs, H., Griffin, R. J., Guzman, M. I., Herrmann, H., Hodzic, A., Iinuma, Y., Jimenez, J. L., Kiendler-Scharr, A., Lee, B. H., Luecken, D. J., Mao, J., McLaren, R., Mutzel, A., Osthoff, H. D., Ouyang, B., Picquet-Varrault, B., Platt, U., Pye, H. O. T., Rudich, Y., Schwantes, R. H., Shiraiwa, M., Stutz, J., Thornton, J. A., Tilgner, A., Williams, B. J., and Zaveri, R. A.: Nitrate radicals and biogenic volatile organic compounds: oxidation, mechanisms, and organic aerosol, Atmos. Chem. Phys., 17, 2103-2162, https://doi.org/10.5194/acp-17-2103-2017, 2017.

Odum, J. R., Hoffmann, T., Bowman, F., Collins, D., Flagan, R. C., and Seinfeld, J. H.: Gas/particle partitioning and secondary organic aerosol yields, Environ. Sci. Technol., 30, 2580-2585, https://doi.org/10.1021/es950943+, 1996.

Pailler, L., Deguillaume, L., Lavanant, H., Schmitz, I., Hubert, M., Nicol, E., Ribeiro, M., Pichon, J. M., Vaïtilingom, M., Dominutti, P., Burnet, F., Tulet, P., Leriche, M., and Bianco, A.: Molecular composition of clouds: a comparison between samples collected at tropical (Réunion Island, France) and mid-north (Puy de Dôme, France) latitudes, Atmos. Chem. Phys., 24, 5567-5584, https://doi.org/10.5194/acp-24-5567-2024, 2024.

Pasquier, J. T., David, R. O., Freitas, G., Gierens, R., Gramlich, Y., Haslett, S., Li, G., Schäfer, B., Siegel, K., Wieder, J., Adachi, K., Belosi, F., Carlsen, T., Decesari, S., Ebell, K., Gilardoni, S., Gysel-Beer, M., Henneberger, J., Inoue, J., Kanji, Z. A., Koike, M., Kondo, Y., Krejci, R., Lohmann, U., Maturilli, M., Mazzolla, M., Modini, R., Mohr, C., Motos, G., Nenes, A., Nicosia, A., Ohata, S., Paglione, M., Park, S., Pileci, R. E., Ramelli, F., Rinaldi, M., Ritter, C., Sato, K., Storelvmo, T., Tobo, Y., Traversi, R., Viola, A., and Zieger, P.: The Ny-Ålesund Aerosol Cloud Experiment (NASCENT): Overview and First Results, Bull. Amer. Meteorol. Soc., 103, E2533-E2558, https://doi.org/10.1175/bams-d-21-0034.1, 2022.

Qi, L., Chen, M., Stefenelli, G., Pospisilova, V., Tong, Y., Bertrand, A., Hueglin, C., Ge, X., Baltensperger, U., Prévôt, A. S. H., and Slowik, J. G.: Organic aerosol source apportionment in Zurich using an extractive electrospray ionization time-of-flight mass spectrometer (EESI-TOF-MS) – Part 2: Biomass burning influences in winter, Atmos. Chem. Phys., 19, 8037-8062, https://doi.org/10.5194/acp-19-8037-2019, 2019.

Rogers, M. J., Joo, T., Hass-Mitchell, T., Canagaratna, M. R., Campuzano-Jost, P., Sueper, D., Tran, M. N., Machesky, J. E., Roscioli, J. R., Jimenez, J. L., Krechmer, J. E., Lambe, A. T., Nault, B. A., and Gentner, D. R.: Humid Summers Promote Urban Aqueous-Phase Production of Oxygenated Organic Aerosol in the Northeastern United States, Geophys. Res. Lett., 52, https://doi.org/10.1029/2024gl112005, 2025.

Roland, D., Barbara, S., Glenn, R., Ariel, S., Albion, T., Sonny, Z., Chris, L., and Alice, C.: HYSPLIT USER's GUIDE, 2025

.

Rolph, G., Stein, A., and Stunder, B.: Real-time Environmental Applications and Display sYstem: READY, Environ. Modell. Softw., 95, 210-228, https://doi.org/10.1016/j.envsoft.2017.06.025, 2017.

Sehested, K., Christensen, H. C., Hart, E. J., and Corfitzen, H.: Rates Of Reaction Of O^-, OH, And H With Methylated Benzenes In Aqueous Solution. Optical Spectra Of Radicals, J. Phys. Chem., 79, 310-315, https://doi.org/10.1021/j100571a005, 1975.

Shen, H., Zhao, D., Pullinen, I., Kang, S., Vereecken, L., Fuchs, H., Acir, I. H., Tillmann, R., Rohrer, F., Wildt, J., Kiendler-Scharr, A., Wahner, A., and Mentel, T. F.: Highly Oxygenated Organic Nitrates Formed from NO_3 Radical-Initiated Oxidation of β-Pinene, Environ. Sci. Technol., 55, 15658-15671, https://doi.org/10.1021/acs.est.1c03978, 2021.

Shen, H. R., Vereecken, L., Kang, S. A., Pullinen, I., Fuchs, H., Zhao, D. F., and Mentel, T. F.: Unexpected significance of a minor reaction pathway in daytime formation of biogenic highly oxygenated organic compounds, Sci. Adv., 8, eabp8702, https://doi.org/10.1126/sciadv.abp8702, 2022.

Shingler, T., Dey, S., Sorooshian, A., Brechtel, F. J., Wang, Z., Metcalf, A., Coggon, M., Mülmenstädt, J., Russell, L. M., Jonsson, H. H., and Seinfeld, J. H.: Characterisation and airborne deployment of a new counterflow virtual impactor inlet, Atmos. Meas. Tech., 5, 1259-1269, https://doi.org/10.5194/amt-5-1259-2012, 2012.

Song, Z., Gao, W., Shen, H., Jin, Y., Zhang, C., Luo, H., Pan, L., Yao, B., Zhang, Y., Huo, J., Sun, Y., Yu, D., Chen, H., Chen, J., Duan, Y., Zhao, D., and Xu, J.: Roles of Regional Transport and Vertical Mixing in Aerosol Pollution in Shanghai Over the COVID-19 Lockdown Period Observed Above Urban Canopy, J. Geophys. Res.-Atmos., 128, https://doi.org/10.1029/2023jd038540, 2023.

Stefenelli, G., Pospisilova, V., Lopez-Hilfiker, F. D., Daellenbach, K. R., Hüglin, C., Tong, Y., Baltensperger, U., Prévôt, A. S. H., and Slowik, J. G.: Organic aerosol source apportionment in Zurich using an extractive electrospray ionization time-of-flight mass spectrometer (EESI-TOF-MS) – Part 1: Biogenic influences and day–night chemistry in summer, Atmos. Chem. Phys., 19, 14825-14848, https://doi.org/10.5194/acp-19-14825-2019, 2019.

Stein, A. F., Draxler, R. R., Rolph, G. D., Stunder, B. J. B., Cohen, M. D., and Ngan, F.: NOAA's HYSPLIT atmospheric transport and dispersion modeling system, Bull. Amer. Meteor. Soc., 96, 2059-2077, https://doi.org/10.1175/BAMS-D-14-00110.1, 2015.

Sun, W., Hu, X., Fu, Y., Zhang, G., Zhu, Y., Wang, X., Yan, C., Xue, L., Meng, H., Jiang, B., Liao, Y., Wang, X., Peng, P. a., and Bi, X.: Different formation pathways of nitrogen-containing organic compounds in aerosols and fog water in northern China, Atmos. Chem. Phys., 24, 6987-6999, https://doi.org/10.5194/acp-24-6987-2024, 2024a.

Sun, W., Fu, Y., Zhang, G., Yang, Y., Jiang, F., Lian, X., Jiang, B., Liao, Y., Bi, X., Chen, D., Chen, J., Wang, X., Ou, J., Peng, P. a., and Sheng, G.: Measurement report: Molecular characteristics of cloud water in southern China and insights into aqueous-phase processes from Fourier transform ion cyclotron resonance mass spectrometry, Atmos. Chem. Phys., 21, 16631-16644, https://doi.org/10.5194/acp-21-16631-2021, 2021.

Sun, W., Zhang, G., Guo, Z., Fu, Y., Peng, X., Yang, Y., Hu, X., Lin, J., Jiang, F., Jiang, B., Liao, Y., Chen, D., Chen, J., Ou, J., Wang, X., Peng, P. a., and Bi, X.: Formation of In-Cloud Aqueous-Phase Secondary Organic Matter and Related Characteristic Molecules, J. Geophys. Res.-Atmos., 129, https://doi.org/10.1029/2023jd040355, 2024b.

Sun, Y., Luo, H., Li, Y., Zhou, W., Xu, W., Fu, P., and Zhao, D.: Atmospheric organic aerosols: online molecular characterization and environmental impacts, npj Clim. Atmos. Sci., 8, https://doi.org/10.1038/s41612-025-01199-2, 2025.

Sun, Y., Du, W., Fu, P., Wang, Q., Li, J., Ge, X., Zhang, Q., Zhu, C., Ren, L., Xu, W., Zhao, J., Han, T., Worsnop, D. R., and Wang, Z.: Primary and secondary aerosols in Beijing in winter: sources, variations and processes, Atmos. Chem. Phys., 16, 8309-8329, https://doi.org/10.5194/acp-16-8309-2016, 2016.

Surdu, M., Top, J., Yang, B., Zhang, J., Slowik, J. G., Prevot, A. S. H., Wang, D. S., El Haddad, I., and Bell, D. M.: Real-Time Identification of Aerosol-Phase Carboxylic Acid Production Using Extractive Electrospray Ionization Mass Spectrometry, Environ. Sci. Technol., https://doi.org/10.1021/acs.est.4c01605, 2024.

Tan, Y., Perri, M. J., Seitzinger, S. P., and Turpin, B. J.: Effects of Precursor Concentration and Acidic Sulfate in Aqueous G

lyoxal-OH Radical Oxidation and Implications for Secondary Organic Aerosol, Environ. Sci. Technol., 43, 8105-8112, https://doi.org/10.1021/es901742f, 2009.

Thomas, A. E., Perraud, V., Lee, M., Rojas, B., Cooke, M. E., Wingen, L. M., Bauer, P. S., Dam, M., Finlayson-Pitts, B. J., and Smith, J. N.: Organic composition of ultrafine particles formed from automotive braking, Environ Sci Process Impacts, https://doi.org/10.1039/d5em00654f, 2025.

Tilgner, A., Schaefer, T., Alexander, B., Barth, M., Collett, J. L., Jr., Fahey, K. M., Nenes, A., Pye, H. O. T., Herrmann, H., and McNeill, V. F.: Acidity and the multiphase chemistry of atmospheric aqueous particles and clouds, Atmos. Chem. Phys., 21, 13483-13536, https://doi.org/10.5194/acp-21-13483-2021, 2021.

Tong, Y., Pospisilova, V., Qi, L., Duan, J., Gu, Y., Kumar, V., Rai, P., Stefenelli, G., Wang, L., Wang, Y., Zhong, H., Baltensperger, U., Cao, J., Huang, R.-J., Prévôt, A. S. H., and Slowik, J. G.: Quantification of solid fuel combustion and aqueous chemistry contributions to secondary organic aerosol during wintertime haze events in Beijing, Atmos. Chem. Phys., 21, 9859-9886, https://doi.org/10.5194/acp-21-9859-2021, 2021.

Volkamer, R., Martini, F. S., Molina, L. T., Salcedo, D., Jimenez, J. L., and Molina, M. J.: A missing sink for gas-phase glyoxal in Mexico City: Formation of secondary organic aerosol, Geophys. Res. Lett., 34, https://doi.org/10.1029/2007gl030752, 2007.

Volkamer, R., Jimenez, J. L., San Martini, F., Dzepina, K., Zhang, Q., Salcedo, D., Molina, L. T., Worsnop, D. R., and Molina, M. J.: Secondary organic aerosol formation from anthropogenic air pollution: Rapid and higher than expected, Geophys. Res. Lett., 33, L17811, https://doi.org/10.1029/2006gl026899, 2006.

Wang, J., Ye, J., Zhang, Q., Zhao, J., Wu, Y., Li, J., Liu, D., Li, W., Zhang, Y., Wu, C., Xie, C., Qin, Y., Lei, Y., Huang, X., Guo, J., Liu, P., Fu, P., Li, Y., Lee, H. C., Choi, H., Zhang, J., Liao, H., Chen, M., Sun, Y., Ge, X., Martin, S. T., and Jacob, D. J.: Aqueous production of secondary organic aerosol from fossil-fuel emissions in winter Beijing haze, Proc. Natl. Acad. Sci. U. S. A., 118, e2022179118, https://doi.org/10.1073/pnas.2022179118, 2021.

Wang, L., Slowik, J. G., Klein, F., Stefenelli, G., Pospisilova, V., Tong, Y., Baltensperger, U., and Prevot, A. S. H.: Characteristics of oxygenated volatile organic compounds in Zurich, Switzerland: Sources, composition, and implication for secondary aerosol formation, Chemosphere, 368, 143686, https://doi.org/10.1016/j.chemosphere.2024.143686, 2024a.

Wang, T., Li, K., Bell, D. M., Zhang, J., Cui, T., Surdu, M., Baltensperger, U., Slowik, J. G., Lamkaddam, H., El Haddad, I., and Prevot, A. S. H.: Large contribution of in-cloud production of secondary organic aerosol from biomass burning emissions, npj Clim. Atmos. Sci., 7, https://doi.org/10.1038/s41612-024-00682-6, 2024b.

Wang, Y., Hu, M., Lin, P., Guo, Q., Wu, Z., Li, M., Zeng, L., Song, Y., Zeng, L., Wu, Y., Guo, S., Huang, X., and He, L.: Molecular Characterization of Nitrogen-Containing Organic Compounds in Humic-like Substances Emitted from Straw Residue Burning, Environ. Sci. Technol., 51, 5951-5961, https://doi.org/10.1021/acs.est.7b00248, 2017.

Wang, Y. Q.: MeteoInfo: GIS software for meteorological data visualization and analysis, Meteorol. Appl., 21, 360-368, https://doi.org/10.1002/met.1345, 2014.

Xu, W., Sun, Y., Wang, Q., Zhao, J., Wang, J., Ge, X., Xie, C., Zhou, W., Du, W., Li, J., Fu, P., Wang, Z., Worsnop, D. R., and Coe, H.: Changes in Aerosol Chemistry From 2014 to 2016 in Winter in Beijing: Insights From High-Resolution Aerosol Mass Spectrometry, J. Geophys. Res.-Atmos., 124, 1132-1147, https://doi.org/10.1029/2018jd029245, 2019.

Xue, S., Luo, H., Wang, Z., Shen, H., Zhang, Y., Nie, C., Song, Z., Wang, L., Wang, S., Chen, J., and Zhao, D.: Online molecular insights into sources and formation of organic aerosol in Shanghai, npj Clim. Atmos. Sci., 8, https://doi.org/10.1038/s41612-025-01230-6, 2025.

Yin, C., Xu, J., Gao, W., Pan, L., Gu, Y., Fu, Q., and Yang, F.: Characteristics of fine particle matter at the top of Shanghai Tower, Atmos. Chem. Phys., 23, 1329-1343, https://doi.org/10.5194/acp-23-1329-2023, 2023.

Yu, L., Smith, J., Laskin, A., George, K. M., Anastasio, C., Laskin, J., Dillner, A. M., and Zhang, Q.: Molecular transformations of phenolic SOA during photochemical aging in the aqueous phase: competition among oligomerization, functionalization, and fragmentation, Atmos. Chem. Phys., 16, 4511-4527, https://doi.org/10.5194/acp-16-4511-2016, 2016.

Zhang, X., Chen, Z. M., and Zhao, Y.: Laboratory simulation for the aqueous OH-oxidation of methyl vinyl ketone and meth

acrolein: significance to the in-cloud SOA production, Atmos. Chem. Phys., 10, 9551-9561, https://doi.org/10.5194/acp-10-9551-2010, 2010.

Zhang, Y., Xu, W., Zhou, W., Li, Y., Zhang, Z., Du, A., Qiao, H., Kuang, Y., Liu, L., Zhang, Z., He, X., Cheng, X., Pan, X., Fu, Q., Wang, Z., Ye, P., Worsnop, D. R., and Sun, Y.: Characterization of organic vapors by a Vocus proton-transfer-reaction mass spectrometry at a mountain site in southeastern China, Sci. Total Environ., 919, 170633, https://doi.org/10.1016/j.scitotenv.2024.170633, 2024.

Zhao, J., Qiu, Y., Zhou, W., Xu, W., Wang, J., Zhang, Y., Li, L., Xie, C., Wang, Q., Du, W., Worsnop, D. R., Canagaratna, M. R., Zhou, L., Ge, X., Fu, P., Li, J., Wang, Z., Donahue, N. M., and Sun, Y.: Organic Aerosol Processing During Winter Severe Haze Episodes in Beijing, J. Geophys. Res.-Atmos., 124, 10248-10263, https://doi.org/10.1029/2019jd030832, 2019.

Zhao, R., Lee, A. K. Y., Huang, L., Li, X., Yang, F., and Abbatt, J. P. D.: Photochemical processing of aqueous atmospheric brown carbon, Atmos. Chem. Phys., 15, 6087-6100, https://doi.org/10.5194/acp-15-6087-2015, 2015.

Zhao, Y., Hallar, A. G., and Mazzoleni, L. R.: Atmospheric organic matter in clouds: exact masses and molecular formula identification using ultrahigh-resolution FT-ICR mass spectrometry, Atmos. Chem. Phys., 13, 12343-12362, https://doi.org/10.5194/acp-13-12343-2013, 2013.

Supplement of

Molecular composition and processing of aqueous secondary organic aerosol in clouds at a mountain site in southeastern China

Yali Jin et al.

Corresponding to: Defeng Zhao (dfzhao@fudan.edu.cn)

Text S1. Meteorological condition and backward trajectories

The temperature (T) of CE1 was the lowest among the four CEs, while the T of CE3 was the highest. In CE2, RH was the highest in four CEs. The air mass of CE1 originated from the southwest of the Shanghuang site. The duration time of CE2 was 22.5 hours, during which the origin of air mass turned from southwest (Fujian and Jiangxi provinces) to north (Mongolia) at 12:00 on May 12th, resulting in a marked decrease in $PM_{2.5}$ concentration. CE3 lasted for 1.5 h, the shortest duration time, so RH and T were more stable. The air mass in CE3 originated from the ocean in the southeast, which is different from other CEs. The duration time of CE4 is 34 h, the longest of all CEs, the air mass of which came from the southwest and turned to the northeast in the second half of the duration time at 17:00 on May 27th.

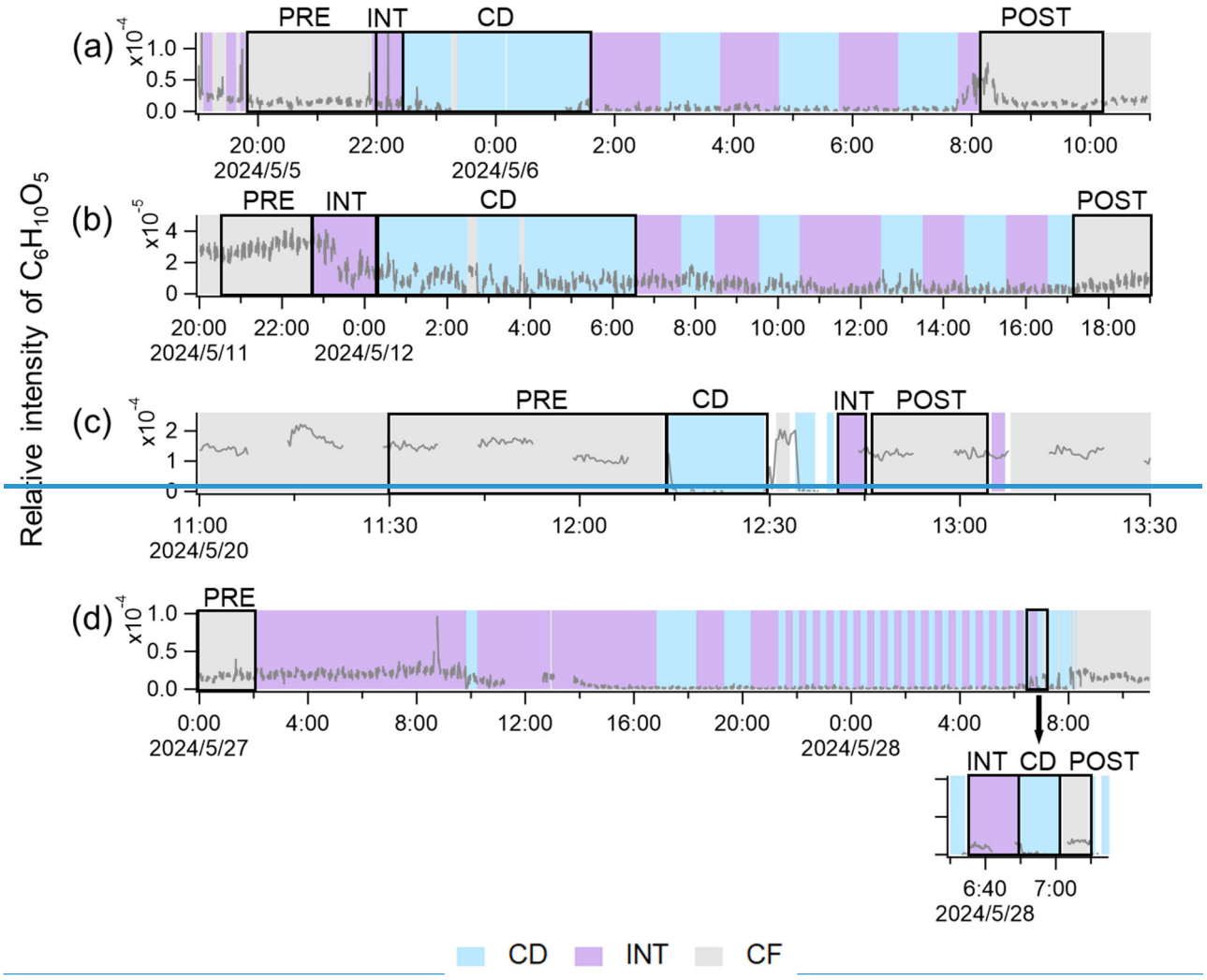
Relative intensity of $C_6H_{10}O_5$
(a)
PRE
INT
CD
POST
x10^-4
1.0
0.5
0.0
20:00
2024/5/5
22:00
0:00
2024/5/6
2:00
4:00
6:00
8:00
10:00
(b)
PRE
INT
CD
POST
x10^-5
4
2
0
20:00
2024/5/11
22:00
0:00
2024/5/12
2:00
4:00
6:00
8:00
10:00
12:00
14:00
16:00
18:00
(c)
PRE
CD
INT
POST
x10^-4
2
1
0
11:00
2024/5/20
11:30
12:00
12:30
13:00
13:30
(d)
PRE
x10^-4
1.0
0.5
0.0
0:00
2024/5/27
4:00
8:00
12:00
16:00
20:00
0:00
2024/5/28
4:00
8:00
INT
CD
POST
6:40
7:00
2024/5/28
CD
INT
CF

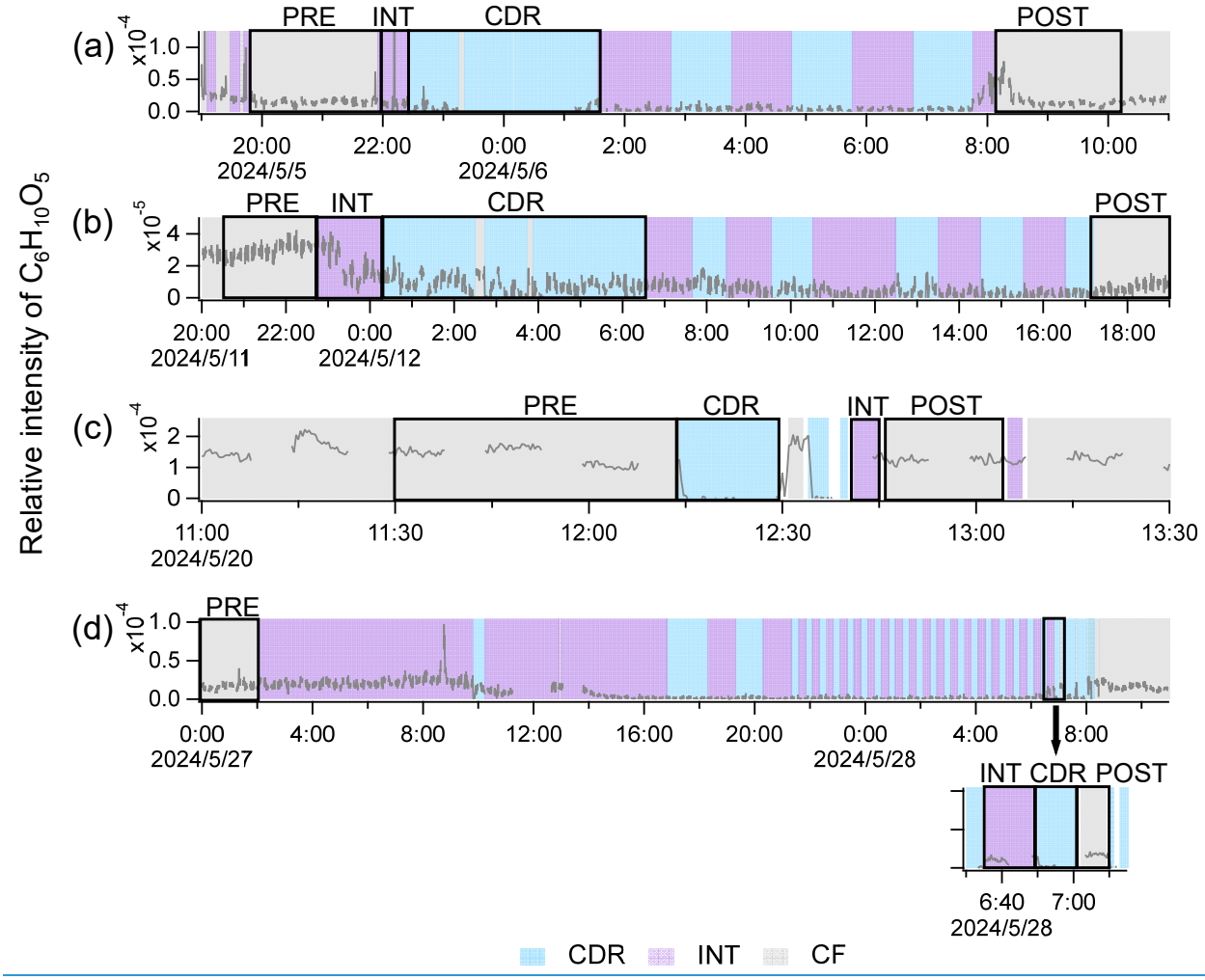

Figure S1. Operational definition of the pre-cloud, in-cloud (including sample types of ~~CD~~CDR and INT) and post-cloud stages in (a) CE1, (b) CE2, (c) CE3, and (d) CE4. Time series of $C_6H_{10}O_5$ is shown as an example. ~~CD~~CDR, INT, and CF samples are shaded in blue, purple, and gray, respectively. Gaps in the time series represent EESI-ToF-MS background measurement periods, which are not shown.

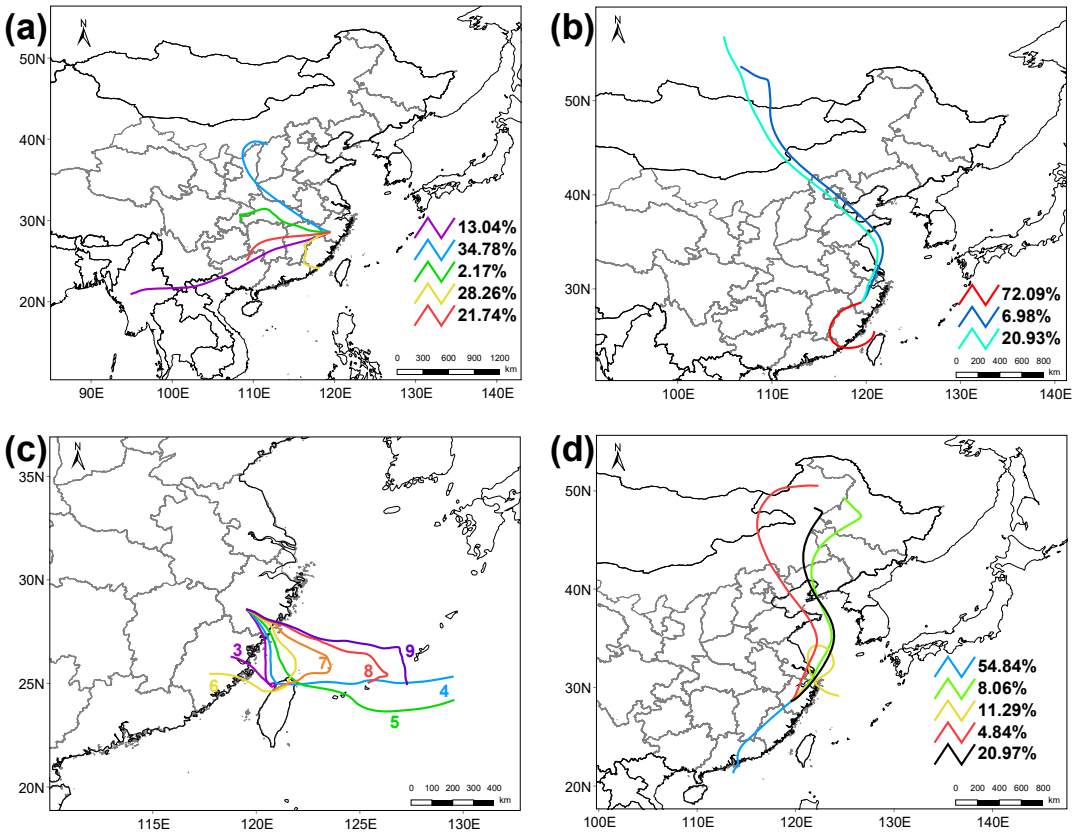

Figure S2. HYSPLIT 3-day backward trajectory analysis of air masses arriving at the Shanghuang site in (a) CE1, (b) CE2, (c) CE3, and (d) CE4. Trajectories are based on cluster analysis for CE1, CE2 and CE4. For CE3, due to its short duration, only 7-hour trajectories are shown with time in UTC.

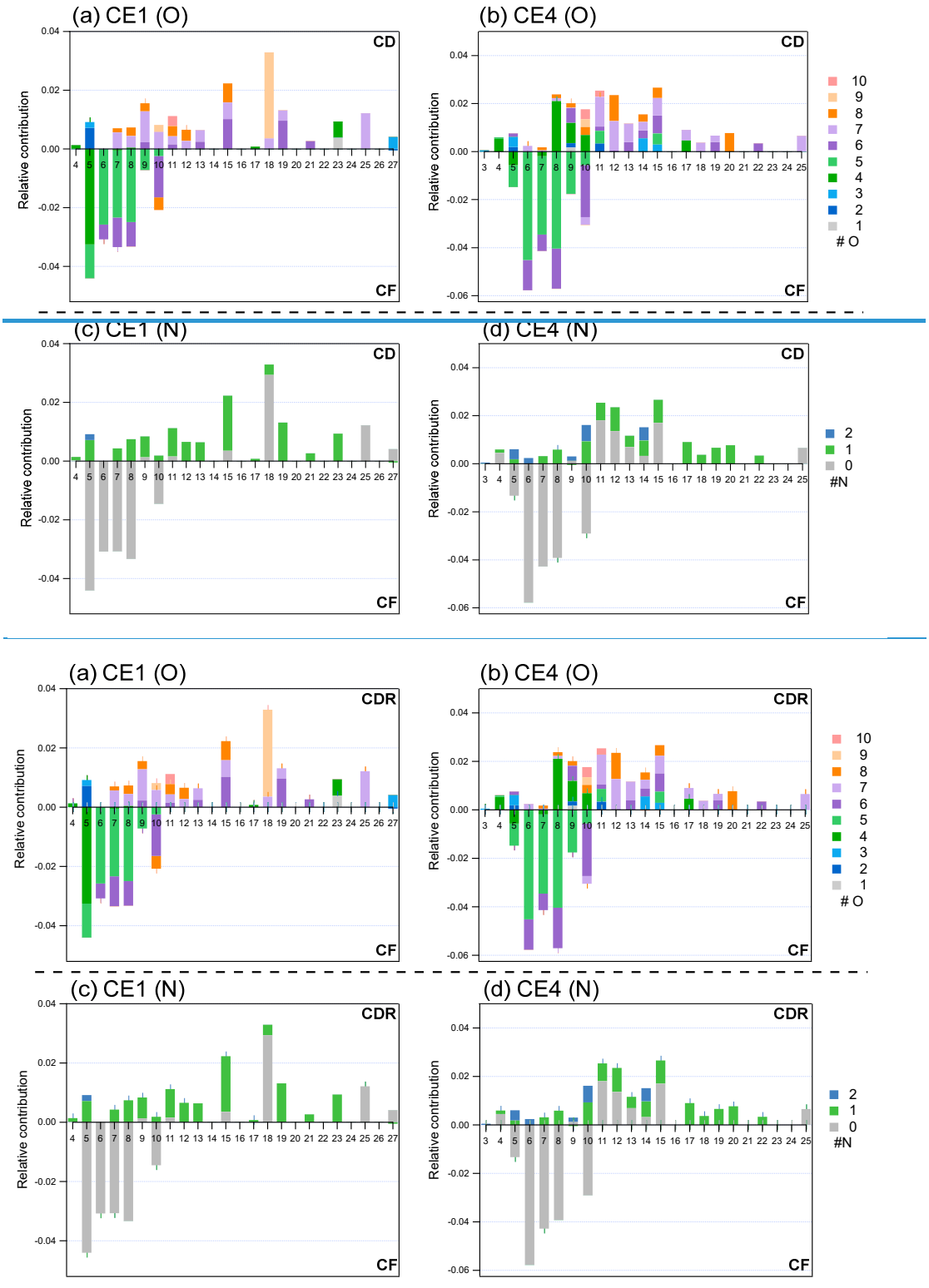

Figure S3. Detailed relative contribution of OA. The average carbon number distribution of differences between ~~CD~~CDR and CF are colored by oxygen number of CE2 (a), CE3 (b); and nitrogen number of CE2 (c), CE3 (d). Positive value stands for significant molecular characteristics of ~~CD~~CDR, and negative value stands for that of CF. Fractions of compounds are normalized to sum of signals of all organics in ~~CD~~CDR and CF, respectively.

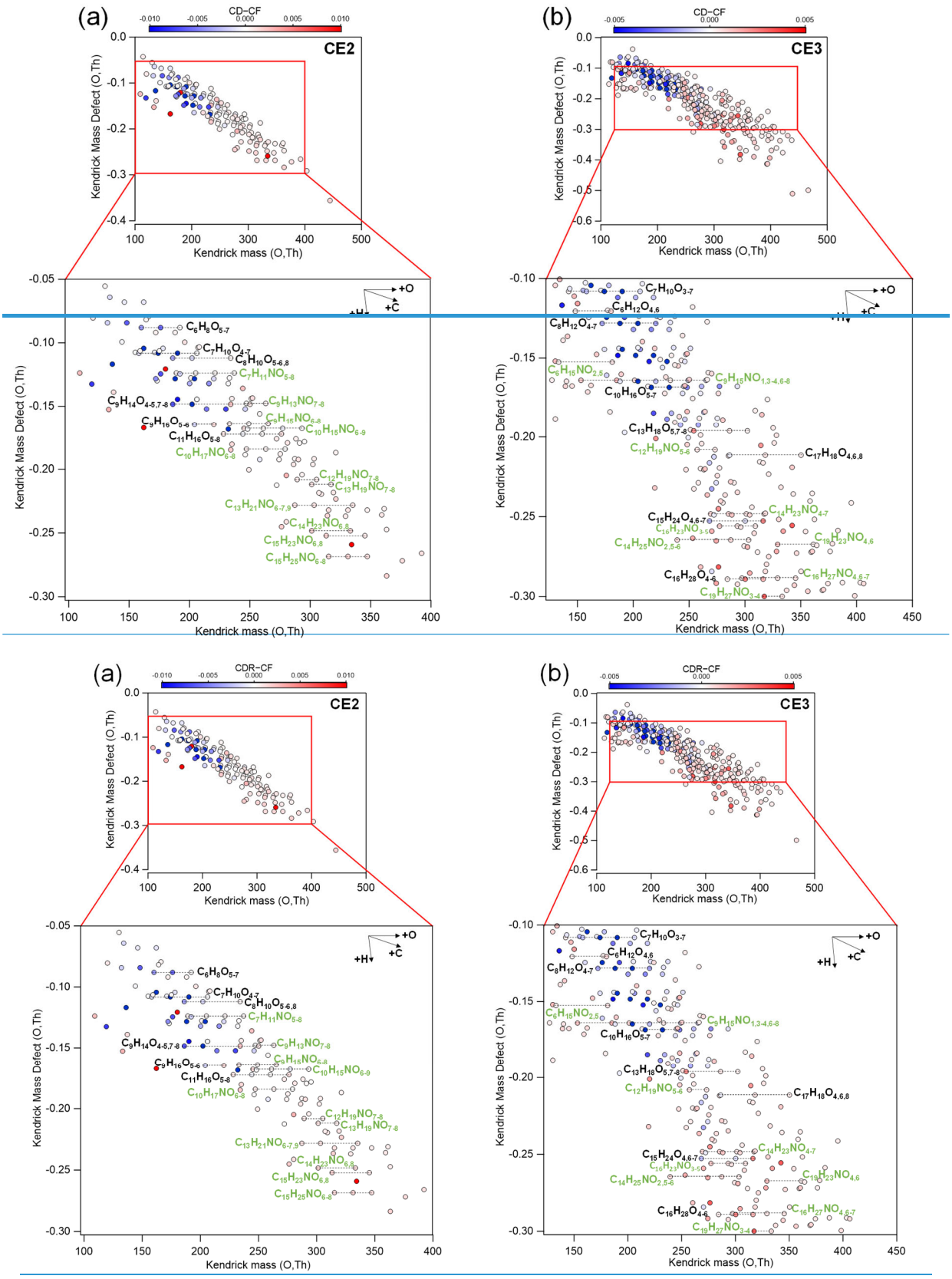

Figure S4. Kendrick mass defect plots based on O of compounds in (a) CE2 and (b) CE3. Data points are color-coded by differences in fraction of compounds between ~~CD~~CDR and CF. Fraction of compounds are normalized to the sum of signals of all organics in ~~CD~~CDR and CF, respectively. Note that, for conciseness, data points in CE3 with normalized signal difference between −0.0003 and 0.0003 (appearing nearly white) are not shown here. Siloxane compounds are not shown here for clarity.

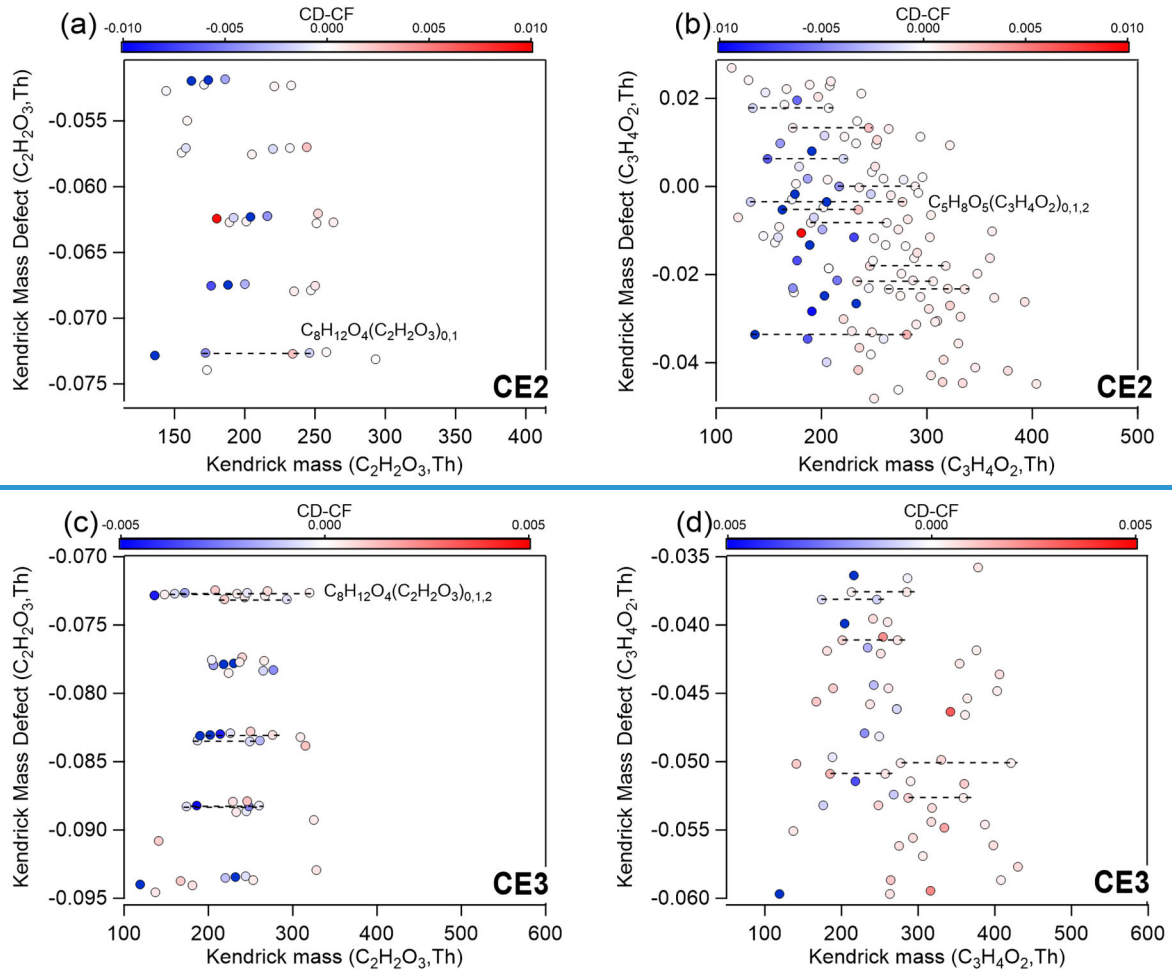
(a)
CD-CF
-0.010
-0.005
0.000
0.005
0.010
Kendrick Mass Defect ($C_2H_2O_3$,Th)
-0.055
-0.060
-0.065
-0.070
-0.075
$C_8H_{12}O_4(C_2H_2O_3)_{0,1}$
CE2
150
200
250
300
350
400
Kendrick mass ($C_2H_2O_3$,Th)
(b)
CD-CF
.010
-0.005
0.000
0.005
0.010
Kendrick Mass Defect ($C_3H_4O_2$,Th)
0.02
0.00
-0.02
-0.04
$C_5H_8O_5(C_3H_4O_2)_{0,1,2}$
CE2
100
200
300
400
500
Kendrick mass ($C_3H_4O_2$,Th)
(c)
CD-CF
-0.005
0.000
0.005
Kendrick Mass Defect ($C_2H_2O_3$,Th)
-0.070
-0.075
-0.080
-0.085
-0.090
-0.095
$C_8H_{12}O_4(C_2H_2O_3)_{0,1,2}$
CE3
100
200
300
400
500
600
Kendrick mass ($C_2H_2O_3$,Th)
(d)
CD-CF
0.005
0.000
0.005
Kendrick Mass Defect ($C_3H_4O_2$,Th)
-0.035
-0.040
-0.045
-0.050
-0.055
-0.060
CE3
100
200
300
400
500
600
Kendrick mass ($C_3H_4O_2$,Th)

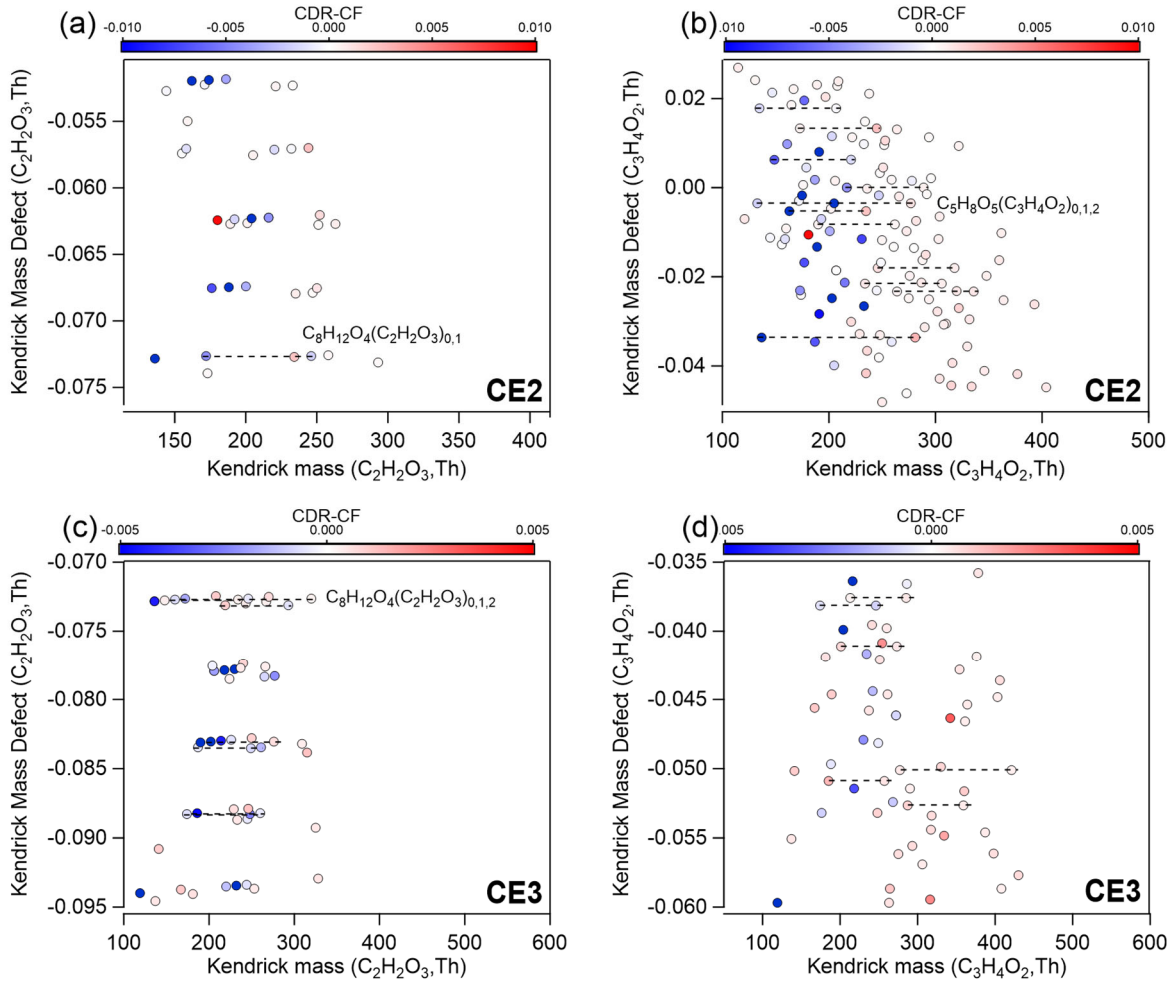

Figure S5. Kendrick mass defect plots based on (a) $C_2H_2O_3$ and (b) $C_3H_4O_2$ of compounds in CE2; and (c) $C_2H_2O_3$ and (d) $C_3H_4O_2$ of compounds in CE3. Data points are color-coded by differences in fraction of compounds between ~~CD~~CDR and CF. Fraction of compounds are normalized to the sum of signals of all organics in ~~CD~~CDR and CF, respectively. Note that, for conciseness, data points in CE3 with normalized signal difference between −0.0003 and 0.0003 (appearing nearly white) are not shown here.

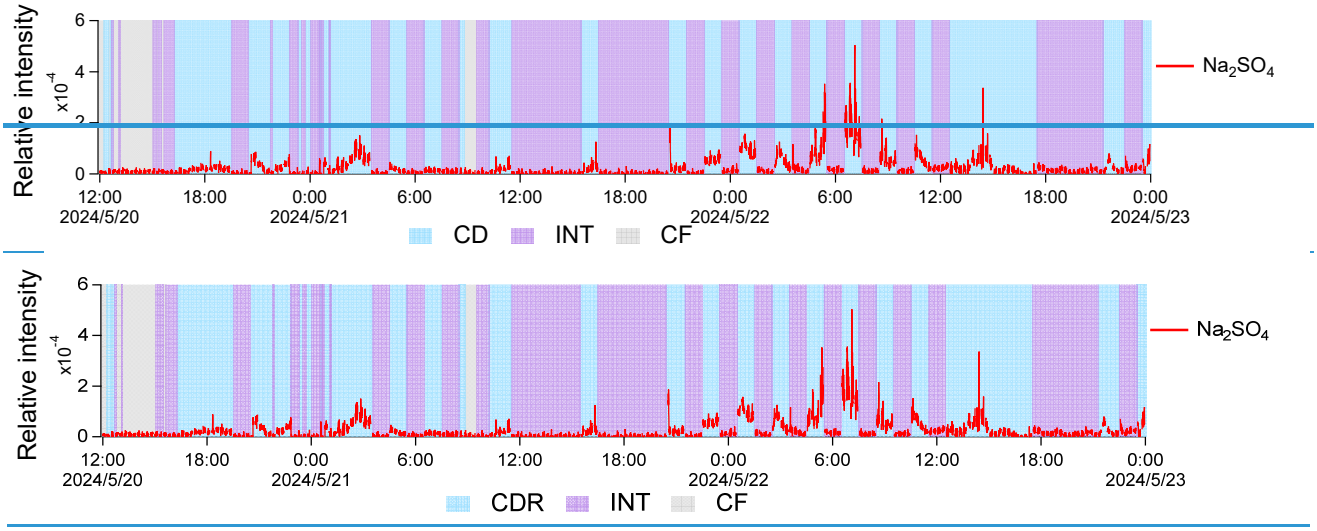

Figure S6. Typical time series of sulfate (Na_2SO_4) in a cloud episode. ~~CD~~CDR, INT, and CF are shaded as blue, purple, and gray, respectively. Gaps in the time series represent EESI-ToF-MS background measurement periods, which are not shown.

Table S1: General characteristics of CE1–CE4, including $PM_{2.5}$ and CO concentration, meteorological parameters (RH and T), origin of air mass, and duration time of each whole cloud episode, respectively. Measured values are shown as mean ± standard deviation.

	CE1	CE2	CE3	CE4
$PM_{2.5}$ (μg m^{-3})	4.3±3.0	5.3±6.7	13.5±1.5	3.8±3.6
CO (ppm)	0.29±0.03	0.26±0.06	0.17±0.002	0.19±0.03
RH (%)	94.7±12.0	97.7±6.7	90.8±5.9	95.0±9.1
T (℃)	15.1±1.7	15.7±3.0	18.0±0.6	17.3±4.0
Origin of air mass	Southwest	Southwest then turns to north	Southeast	Southwest then turns to northwest
Duration time (hour)	14	22.5	1.5	34

Table S2: Mean atom numbers (n_C, n_H, n_O, and n_N; mean ± standard deviation) of OA for CE1–CE4 in pre-cloud aerosols, ~~CD~~CDR, INT, and post-cloud aerosols.

		Pre-cloud aerosols	~~CD~~CDR	INT	Post-cloud aerosols
CE1	n_C	8.72±0.38	10.45±1.07	8.99±0.53	8.86±0.41
	n_H	13.81±1.09	17.25±3.16	14.21±1.17	14.45±1.10
	n_O	5.64±0.12	6.02±0.33	5.68±0.13	5.71±0.15
	n_N	0.20±0.03	0.32±0.08	0.26±0.05	0.22±0.04
CE2	n_C	8.33±0.20	10.13±1.26	8.52±0.34	11.12±0.55
	n_H	13.72±0.65	19.51±4.50	14.19±1.05	21.10±2.80
	n_O	4.98±0.12	5.44±0.57	4.92±0.18	6.26±0.20
	n_N	0.28±0.04	0.39±0.09	0.33±0.07	0.33±0.07
CE3	n_C	10.57±0.18	12.92±0.70	10.42±0.09	10.51±0.13
	n_H	16.14±0.30	21.78±1.76	16.21±0.20	16.18±0.29
	n_O	5.08±0.05	5.15±0.12	5.09±0.03	5.11±0.04
	n_N	0.30±0.02	0.42±0.06	0.27±0.02	0.27±0.02
CE4	n_C	8.17±0.15	9.95±0.49	8.94±0.20	8.77±0.12
	n_H	12.99±0.19	14.53±0.65	13.36±0.26	13.20±0.17
	n_O	5.29±0.08	5.68±0.23	5.52±0.08	5.52±0.06
	n_N	0.12±0.03	0.32±0.08	0.20±0.04	0.18±0.02

Table S3: Compounds with larger fraction in ~~CD~~CDR than CF in CE1, CE2, CE3, and CE4.

	Formula			
CE1	C4H4NO4	C8H13NO7	C10H17NO6	C15H23NO8
	C4H6O5	C8H13NO8	C10H17NO7	C15H25NO8
	C5H13NO2	C8H14O6	C11H16O6	C17H13NO4
	C5H8N2O3	C9H12O6	C11H17NO7	C18H19NO7
	C5H12O4	C9H12O7	C11H19NO8	C18H23NO7
	C6H4O5	C9H13NO7	C11H23NO10	C18H54O9Si9
	C6H10O6	C9H14O7	C12H19NO7	C19H25NO7
	C7H8O5	C9H15NO7	C12H19NO8	C19H23NO6
	C7H8O6	C9H15NO8	C13H15NO6	C21H31NO6
	C7H10O7	C10H13NO8	C13H19NO7	C23H17NO
	C7H11NO7	C10H14O7	C15H25NO6	C23H21NO4
	C7H11NO8	C10H15NO7	C15H25NO7	C25H32O7
	C8H6O4	C10H15NO8	C15H15O6	C27H20O3
	C8H10O6	C10H15NO9	C15H15NO7	
	C8H11NO7	C10H16O7	C15H23NO6	
CE2	C3H2N2O3	C9H8O5	C11H18O6	C14H23NO6
	C4H4NO4	C9H12O6	C11H19NO8	C14H23NO8
	C4H8O4	C9H13NO7	C11H20O8	C15H19NO6
	C6H8O7	C9H13NO8	C11H23NO10	C15H25NO6
	C6H9NO7	C9H14O7	C12H12O6	C15H25NO7
	C6H12O6	C9H14O8	C12H16O7	C15H15O6
	C6H15NO2	C9H15NO6	C12H16O8	C15H15NO7
	C7H8O5	C9H15NO7	C12H17NO7	C15H17N3O5
	C7H8O6	C9H15NO8	C12H17NO8	C15H21NO9
	C7H11N	C9H16O6	C12H18O7	C15H22O7
	C7H11NO5	C9H17NO6	C12H18O8	C15H23NO6
	C7H11NO6	C10H8O5	C12H19NO7	C15H23NO8
	C7H11NO7	C10H12O7	C12H19NO8	C15H25NO8
	C7H11NO8	C10H15NO6	C12H24O7	C16H19NO6
	C7H11N3	C10H15NO7	C13H19NO8	C16H48O8Si8
	C7H13N2SO	C10H15NO9	C13H15NO6	C17H13NO4
	C8H6O4	C10H14N2	C13H18O7	C17H22N2O5
	C8H10O8	C10H17NO6	C13H18O8	C18H19NO7
	C8H11NO5	C10H17NO7	C13H19NO7	C18H21NO7
	C8H11NO7	C10H17NO8	C13H20O6	C18H54O9Si9
	C8H14O6	C10H18O6	C13H21NO6	C19H17NO3
	C8H13NO7	C10H19NO6	C13H21NO7	C19H25NO6
	C8H13NO8	C11H14O7	C13H21NO9	C20H24O7
	C8H14O6	C11H16O5	C13H24O6	C21H25NO7
	C9H7N2O	C11H16O7	C14H21NO7	C25H32O7
	C9H7N2O2	C11H16O8	C14H21NO8	C27H20O3
	C9H8SO	C11H17NO7	C14H21NO9	
CE3	C4H7NO3	C12H10O7	C15H22O5	C19H18O6
	C4H7N3O3	C12H13NO6	C15H22O4	C19H19NO2
	C4H8O4	C12H14O7	C15H24O7	C19H20O7
	C4H9N3O3	C12H15NO5	C15H26O6	C19H22O5
	C5H10O4	C12H16O10	C15H26O6	C19H22O7
	C5H12O4	C12H19NO5	C15H28O6	C19H23NO4
	C5H10O4	C12H19NO6	C15H32O7	C19H23NO6
	C6H4SO3	C12H21NO6	C16H23NO5	C19H24O7

	Formula			
	C6H10O3	C12H24O7	C16H25NO5	C19H26O4
	C6H11NO5	C12H36O6Si6	C16H27NO4	C19H26O6
	C6H12O4	C13H12O5	C16H27NO6	C19H28O6
	C6H12O6	C13H14O5	C16H27NO7	C19H29O8
	C6H14N2	C13H14O6	C16H29NO5	C19H31NO6
	C6H14N2O	C13H15N3O7	C16H33NO6	C19H38O5
	C6H15NO2	C13H18O7	C16H15NO	C19H39NO4
	C6H15NO5	C13H17NO4	C16H19NO6	C20H29NO5
	C6H15N3O	C13H18O5	C16H22O4	C20H12N2
	C6H17N3O3	C13H18O8	C16H22O9	C20H14N2O2
	C7H10O3	C13H20O6	C16H23NO3	C20H22O5
	C7H11N3	C13H19NO6	C16H23NO4	C20H24O4
	C7H12O8	C13H22O7	C16H24O5	C20H24O6
	C7H15N2	C13H21NO6	C16H25NO8	C20H24O7
	C7H18N2	C13H22O5	C16H26O8	C20H30O10
	C8H15NO4	C13H24O6	C16H28O4	C20H32O9
	C8H4O3	C14H15NO7	C16H28O5	C20H35NO7
	C8H5NO4	C14H23NO7	C16H28O6	C20H36O5
	C8H7NO	C14H7NO4	C16H32O10	C21H21NO6
	C8H13O2	C14H14O4	C17H33NO4	C21H25NO7
	C8H13NO6	C14H16O4	C17H33NO5	C21H22O5
	C8H15N2	C14H16O5	C17H37N5	C21H23NO2
	C9H7NO2	C14H16N2O3	C17H11N	C21H25NO6
	C9H10O2	C14H19NO7	C17H18O6	C21H26O6
	C9H10O2	C14H20O8	C17H18O8	C21H26O8
	C9H13NO2	C14H21NO	C17H22O5	C21H27NO8
	C9H14O7	C14H22O4	C17H22N2O	C21H28O8
	C9H15NO	C14H23NO4	C17H22N2O5	C21H34O2
	C9H15NO3	C14H23NO5	C17H24O5	C21H38O5
	C9H15NO4	C14H23NO6	C17H26N2O	C22H33NO4
	C9H15NO6	C14H24O6	C17H27NO3	C22H26O5
	C9H16O	C14H24O7	C17H28O7	C22H34O7
	C9H19S	C14H25NO2	C17H29NO	C22H38O6
	C10H12O7	C14H25NO5	C17H29NO7	C23H39NO4
	C10H12N2O4	C14H25NO6	C18H25NO4	C23H22O5
	C10H13NO6	C14H26O5	C18H27NO5	C23H26O6
	C10H15NO4	C14H28O5	C18H29NO6	C24H29NO4
	C10H14N2	C14H28O4	C18H16O6	C24H28O5
	C10H20O5	C14H31N3O10	C18H20O6	C24H50O8
	C11H12O4	C15H21NO8	C18H22O5	C25H17NO4
	C11H16O5	C15H25NO5	C18H23N	C26H29O6
	C11H16O8	C15H12O3	C18H27NO7	C26H29NO
	C11H17NO6	C15H11NO2	C18H28O7	C27H38O2
	C11H19NO6	C15H13N3O5	C18H35NO5	C27H50O4
	C11H20O6	C15H15NO2	C18H35N3O8	C28H24O2
	C11H20N2O5	C15H18O8	C18H54O9Si9	
	C11H21NO5	C15H19NO4	C19H27NO3	
	C11H21NO6	C15H20O4	C19H27NO4	
CE4	C3H2N2O3	C9H8SO	C11H16O5	C14H23NO8
	C4H4NO4	C9H8O5	C11H16O6	C15H25NO6
	C4H6O5	C9H10O6	C11H16O7	C15H25NO7

	Formula			
	C4H8O4	C9H12O6	C11H17NO7	C15H12O3
	C5H13NO2	C9H12O4	C11H18O6	C15H15O6
	C5H6O5	C9H12O7	C11H23NO10	C15H20O5
	C5H6O6	C9H13NO7	C12H16O7	C15H22O7
	C5H8N2O3	C9H13NO8	C12H16O8	C15H23NO6
	C5H10O4	C9H14O8	C12H17NO7	C15H23NO8
	C5H12O4	C9H16O6	C12H18O6	C15H25NO8
	C6H10N2O7	C10H8O5	C12H18O7	C17H13NO4
	C7H8O6	C10H12N2O4	C12H18O8	C17H19NO7
	C7H10O7	C10H13NO8	C12H19NO7	C18H19NO7
	C7H11NO6	C10H15NO6	C12H19NO8	C18H21NO7
	C7H11NO8	C10H15NO7	C12H24O7	C18H23NO7
	C7H12O6	C10H15NO8	C13H12O6	C19H25NO7
	C8H12O4	C10H15NO9	C13H18O7	C19H23NO6
	C8H14O5	C10H17NO6	C13H19NO7	C20H31NO8
	C8H14O6	C10H17NO7	C13H20O6	C20H33NO8
	C8H13NO7	C10H18O5	C14H15NO7	C22H25NO6
	C8H13NO8	C10H20O10	C14H21NO8	C25H32O7
	C8H14O6	C11H9NO2	C14H16N2O3	
	C9H7N2O2	C11H14O7	C14H20O6	

Note: Duplicated molecular formulas originate from different ion adducts from the ionization of EESI-ToF-MS.